AVS Quantum Science ROADMAP scitation.org/journal/aqs

Technology roadmap for cold-atoms based quantum inertial sensor in space

Cite as: AVS Quantum Sci. **5**, 019201 (2023); doi: 10.1116/5.0098119
Submitted: 5 May 2022 · Accepted: 22 November 2022 ·
Published Online: 20 March 2023

Sven Abend,[1] Baptiste Allard,[2] Aidan S. Arnold,[3] Ticijana Ban,[4] Liam Barry,[5] Baptiste Battelier,[6] Ahmad Bawamia,[7] Quentin Beaufils,[8] Simon Bernon,[6] Andrea Bertoldi,[6] Alexis Bonnin,[9] Philippe Bouyer,[6,10,11,12,13] Alexandre Bresson,[9] Oliver S. Burrow,[3] Benjamin Canuel,[6] Bruno Desruelle,[13] Giannis Drougakis,[14] René Forsberg,[15] Naceur Gaaloul,[1] Alexandre Gauguet,[2] Matthias Gersemann,[1] Paul F. Griffin,[3] Hendrik Heine,[1] Victoria A. Henderson,[16] Waldemar Herr,[1,17] Simon Kanthak,[18] Markus Krutzik,[7,18] Maike D. Lachmann,[1] Roland Lammegger,[19] Werner Magnes,[20] Gaetano Mileti,[21] Morgan W. Mitchell,[22] Sergio Mottini,[23] Dimitris Papazoglou,[14] Franck Pereira dos Santos,[24] Achim Peters,[16] Ernst Rasel,[1] Erling Riis,[3] Christian Schubert,[1,17] Stephan Tobias Seidel,[25] Guglielmo M. Tino,[26] Mathias Van Den Bossche,[23] Wolf von Klitzing,[14] Andreas Wicht,[7] Marcin Witkowski,[27] Nassim Zahzam,[9] and Michał Zawada[27]

For affiliations, please see the end of the Reference section.

Note: This paper is part of the special topic collection, Quantum Sensing as a Technology.

ABSTRACT

Recent developments in quantum technology have resulted in a new generation of sensors for measuring inertial quantities, such as acceleration and rotation. These sensors can exhibit unprecedented sensitivity and accuracy when operated in space, where the free-fall interrogation time can be extended at will and where the environment noise is minimal. European laboratories have played a leading role in this field by developing concepts and tools to operate these quantum sensors in relevant environment, such as parabolic flights, free-fall towers, or sounding rockets. With the recent achievement of Bose–Einstein condensation on the International Space Station, the challenge is now to reach a technology readiness level sufficiently high at both component and system levels to provide "off the shelf" payload for future generations of space missions in geodesy or fundamental physics. In this roadmap, we provide an extensive review on the status of all common parts, needs, and subsystems for the application of atom-based interferometers in space, in order to push for the development of generic technology components.

TABLE OF CONTENTS

I. INTRODUCTION

A. Cold atoms in space: Brief history

Nobel prize awarded achievements, such as laser cooling[1–3] and Bose–Einstein condensation,[4,5] marked the beginnings of national and international initiatives for cold-atom based science in space. Proposals for clocks exploiting laser-cooled atoms, like PHARAO/ACES,[6] pioneered the field, followed by proposals exploiting cold-atom based interferometers, such as HYPER[7] for mapping the Lense–Thirring effect and experiment proposals with Bose–Einstein condensates (BECs). Exploiting atom interferometry in extended free fall for inertial quantum sensing is still one of the biggest drivers for space developments in the field of quantum technologies (Fig. 1 shows a timeline with the most significant cold atoms experiments in space). Atom interferometers (AIs) are proposed for advancing current quests in fundamental physics, for Earth and planetary observation, as well as for space navigation. Benefiting from the progress in the field, an impressive list of milestones has been achieved, which includes, among others, dual-species interferometry on parabolic flights (ICE project[8]), Bose–Einstein condensation and interferometry with BECs in space (MAIUS mission[9]), as well as the first experiments with BECs in NASA's Cold Atom Laboratory (CAL).[10] The next immediate steps in preparation range from sounding rocket missions to a new NASA-DLR Bose–Einstein Condensate Cold Atomic Laboratory (BECCAL) for the International Space Station (ISS) and the Cold Atom Physics Rack (CAPR) on the Chinese space station.[11] These platforms aim at performing quantum gas and interferometry experiments in space using two atomic species, potassium and rubidium. These experiments highlight the maturity of the tools and methods and offer a relatively simple implementation within a few years, which represents an excellent starting condition for space activities. In this game, Europe plays a leading role with access to many microgravity facilities, such as drop towers, Einstein elevators, the ISS, satellites, or new orbital platforms.

B. Motivation for the use of atom sensors in space

The typical sensitivity of atom interferometers to inertial accelerations scales as the square of the interrogation time $2T$. Since during this interrogation, the atoms are in free-fall, ground-based atom interferometric experiments are fundamentally limited by the accessible size of the experiments. This is because an increasing time in free-fall implies an increasing path-length for the atom trajectory—making the control of systematic effects extremely challenging. An attractive alternative to increase $2T$ is to operate the atom interferometer with the whole apparatus in free fall, in space or in a specific microgravity environment.[12–14]

Earth-based cold-atom experiments performed on 0 g can exploit ground based microgravity facilities, such as the 0 g aircraft (the ICE experiment) and the ZARM drop tower (the QUANTUS experiments). The main requirement in these experiments is a very compact and robust design, which must withstand extreme environmental conditions, such as the vibrational noise onboard the plane, or the ∼50 g deceleration during capsule recapture in the tower. The microgravity phase lasts between 5 and 20 s, and measurements can be carried out only during these time intervals. Between repetitions of the 0 g phase, the experiments can have long downtimes (e.g., two to three drops per day for QUANTUS, two flight campaigns per year for ICE). Furthermore, the quality of microgravity in these Earth-based systems is not perfect (∼0.01 g fluctuations during parabolic flights).

In contrast, performing an experiment onboard a satellite offers the possibility of extremely long $2T$ with continuous free-fall operation. In principle, under these conditions, $2T$ would be limited only by the time the cloud of atoms expands, as a consequence of their temperature, before they leave the interrogation area. For example, for an atomic interferometer with ultracold ^{87}Rb atoms at 10 nK and an AI interrogation beam diameter of 2.5 cm, the most probable time for an atom to exit the interrogation area is ∼10 s in the absence of gravity. Operating AIs in space would lead to acceleration sensitivities below 10^{-12} g/$\sqrt{\text{Hz}}$ with interrogation times T of 1 s or more. This level of sensitivity could enable a test of the weak equivalence principle (WEP) on quantum objects[8,15–17] of a few parts in 10^{15}, if we consider integration of the signal over a few weeks. Several developing projects within the ESA, the French space agency (CNES) and the German Aerospace

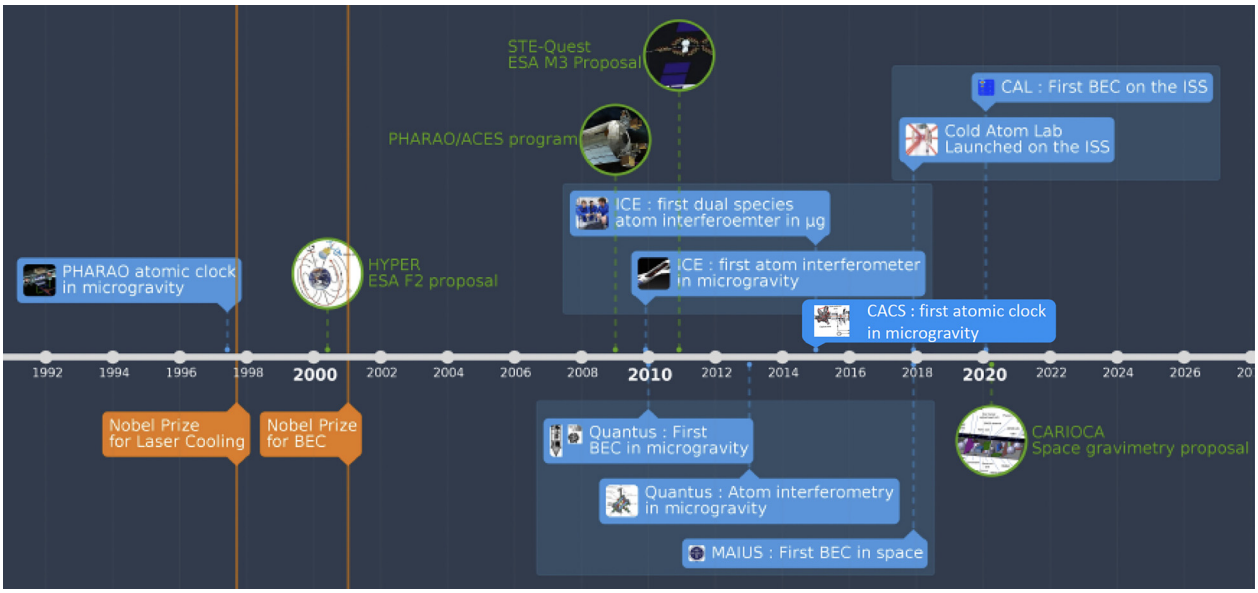

FIG. 1. Brief history of cold atom experiments performed in microgravity and space and of some missions pre-selected by European space agencies.

Center (DLR), are today investigating the potential of cold atom interferometry for precision measurements and fundamental tests in space.

C. Primary applications of atom interferometry in earth observation

The development of atom interferometers for precision measurements and fundamental tests in space can lead to target accuracy at 10^{-15} g and target sensitivity at 10^{-12} g/$\sqrt{\text{Hz}}$. This opens opportunities for applications in remote sensing of the earth's gravity field and its changes in space and time.[18] Measurement of gravity from space is one of the tools for Earth observation (EO). It gives information about the inside structure of the earth via the determination of the geoid (the equipotential surface corresponding to mean sea level) and has important applications in geophysics, for the exploration of minerals, oil, and gas, for precise height determination (with GNSS satellites), as well as for inertial navigation at high accuracy.[19] The measurement of the space-time variations of the gravity field has even more societal applications in climate change, global sea level rise, hydrology, droughts and flooding, global geodynamics, and monitoring earthquakes or volcanic eruptions.

The successful NASA/DLR GRACE and GRACE-FO satellite missions have mapped the time changes of the gravity field since 2002 and uniquely confirmed ability to monitor floods and quantified melt of glaciers and ice sheets to levels not previously possible;[20] the ESA Gravity field and Ocean Circulation Explorer (GOCE) mission from 2009 to 2013 determined the hitherto best spatial resolution gravity field models, significantly improving geodetic surveys across the globe, the understanding of deep earth structures, and the global ocean circulation.[21]

There is a strong societal push to continue these missions, with user needs pointing to higher accuracy and resolution in space and time, both of which are strongly related not only to the accuracy of accelerometers and gradiometers but also to the launch of satellite constellations at challenging low orbit environments. GOCE operated its advanced electrostatic six-axis gradiometer system down to 225 km orbit height, while GRACE/GRACE-FO flies at 480 km nominal orbit height, giving serious limitations in spatial resolution of key user needs, such as near-real time flood monitoring. It is obvious in the long run that quantum technologies can provide breakthrough solutions to the geodesy EO domain.

There is, thus, a need for continued experiments at lab level, airborne and 0 g environments, and through early demonstration in pathfinder satellite missions. Airborne demonstrations of cold atom gravimeter in aircraft have recently proved accuracy of gravity surveys superior to classical gravimeters,[22] due to their inherent absolute accuracy; the measurement does not require any calibrations, potentially solving many past and future problems of gravity field mapping both for geophysical, geodetic, and military applications.

D. Context

1. National and international initiatives

Quantum sensors, and more generally quantum technologies, have gained significant interests in the last few decades with the midst of a second Quantum revolution. Spurred by the spectacular progress in our ability to control and manipulate single and complex quantum objects, this technology is now entering a new phase in developing and commercializing applications, such as Quantum Computing, Communications, and Sensors. The global quantum effort is continually rising with worldwide investments in quantum research and quantum technology reaching almost 25×10^9 dollars on a decade timescale, including public and private funding (see Fig. 2). This global effort is leading to relentless achievements in research and innovation that are continuously furthering the quantum landscape. At the scale of Europe, the Quantum Flagship is aiming to strengthen European scientific leadership and excellence in quantum research and turn

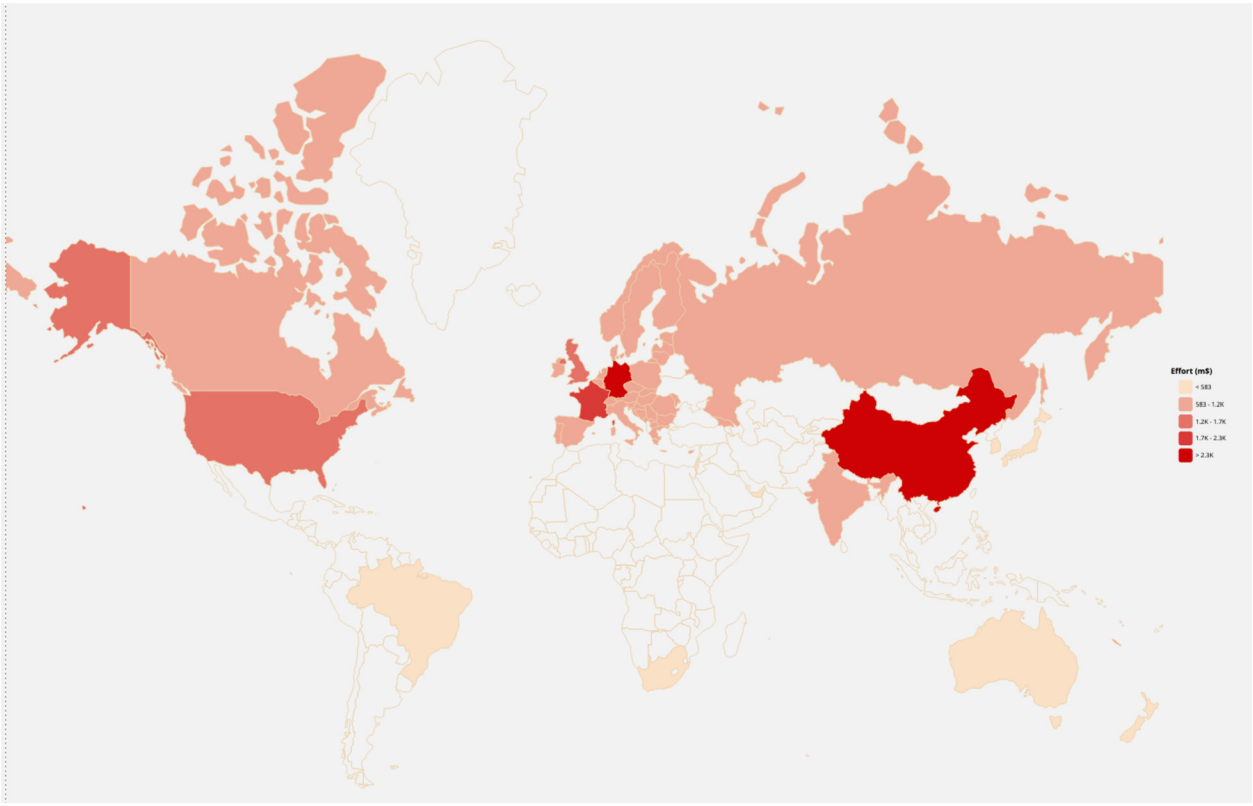

FIG. 2. Overview of funding level in quantum technologies (data taken from Quantum resources and careers[23]).

results into concrete technological opportunities that can be transferred to the industry. This flagship program, led by a high-level group of experts, is a large-scale initiative funded at the 1 b€ level on a 10-year timescale. It consists in a coherent set of research and innovation projects selected through a thorough peer-review process. Calls for projects are issued based on the Flagship's Strategic Research Agenda, thus ensuring that all actors are aligned in the pursue of the Flagship's goals. Many national initiatives complement the overall European Quantum Flagship.[23]

Beyond the EU initiative, many European countries announced very strong commitment in the development of quantum technologies:

- UK has shown increasing participation in quantum research and development. The UK began its first five-year phase in 2015, and after its success, announced the second five-year phase at the end of 2019.
- In 2018, the German Federal Government announced a Framework Program to bring quantum technologies to market. In July 2020, the German government announced a 2 b€ quantum effort, supplementing the EU Quantum Flagship in investment through 2028.
- The Netherlands published in 2019 a National Agenda on Quantum Technologies with four areas of focus in quantum and founded QuTech, the quantum technology institute of the TU Delft (Delft University of Technology) and TNO (Netherlands Organisation for Applied Scientific Research). The Dutch Ministry of Economic Affairs has also announced that they have allocated 615 M€ to Quantum Delta NL in order to aid the advancement of quantum technology.
- France has been investing in quantum technologies every year for decades. The French government recently launched a plan to structure a national strategy for quantum technologies, and in January 2021, French President Emmanuel Macron announced a five-year investment plan worth 1.8 b€ in quantum technologies.
- Since 2006, Italian Space Agency has taken benefit of its MLRO (Matera Laser Ranging Observatory) facility to develop and test technologies for future satellite quantum communications. Since 2013, the Italian Quantum Backbone (IQB) runs through 1850 km of optical fiber. An initiative on quantum gravimetry concepts started in 2016 with the MOCASS study (Mass Observation with Cold Atom Sensors in Space) and the current MOCAST+ evolution. The Italian Government has announced a new phase of investments to make quantum technologies, from sensing to computing, a research priority for the coming years, in co-operation with the European Flagship.

2. Microgravity and space initiatives

The last decades also witnessed many initiatives specifically dedicated to the development of quantum sensors in space. This includes potential pathfinder or dedicated space missions that could lead to technological or scientific breakthroughs. The initial focus was put on

relatively low performance demonstrations of cold atom sensors devices on "ground based" microgravity platforms, like the ESA led *Space Atom Interferometer* program which federated, in 2010, the scientific community through the development of earth prototypes of key components and mockup sensor.[24] Two other programs were led by CNES and DLR over the last 15 years, with important demonstrations in relevant microgravity environment: the ICE program in the 0 g airbus and the QUANTUS program in the ZARM free-fall tower followed by the MAIUS sounding rockets program. Today, ultracold atoms can be produced in space, on the ISS thanks to the CAL (Cold Atom Laboratory) launched by NASA in 2017. This program will be followed by a Chinese equivalent, CCAL and a US/German new platform aiming at quantum sensors demonstrations, BECCAL.

a. QUANTUS/MAIUS and ICE experiments. More than 15 years ago, the DLR started an activity to develop an experiment for generating and investigating Bose–Einstein condensates in microgravity. The major motivation was exploring the potential of space-borne matter-wave interferometry. In this frame, two apparatus, QUANTUS-1 and -2 (see Fig. 3, left), have been built, which are still in operation. They allowed to reach milestones, such as the creation of the first BEC in microgravity, the demonstration of the first BEC interferometer in free fall, delta-kick collimation, as well as the first catapult experiments with BECs demonstrating the high-flux of the QUANTUS-2 experiment. The source concept of QUANTUS-2 paved the way for the sounding rocket mission MAIUS-1 which created, in early 2017, the first BEC in space, exploited its macroscopic coherence, and established space matter-wave interferometry. MAIUS-2 and -3 will allow for experiments with potassium and rubidium, clearing the path for the BECCAL apparatus, a joint endeavor by NASA and DLR.

ICE (see Fig. 3, right), also initiated 15 years ago, was primarily set up to develop a mobile dual-species inertial sensor able to measure the Eötvös parameter η at high precision in a weightless environment, such as that generated onboard the Novespace Zero-g aircraft. Performing WEP tests in this type of environment serves as a proof-of-concept toward using cold-atom technology onboard a satellite, as proposed by the STE-QUEST mission project,[25] where future tests at the 10^{-15} level could become a reality. ICE allowed to push the technology and the operation of cold-atom sensors in weightlessness using this specific free falling vehicle.[26]

b. Cold atoms on space station experiments. The NASA Cold Atom Laboratory operates, since June 2018, a multi-user BEC facility on board the ISS.[10,27] Selected researchers explore, with this atom-chip-based payload, cold matter physics through a remote operation by the Jet Propulsion Laboratory team. Experiments involving the transport, collimation, and interferometry of BECs are conducted. Moreover, atom interferometry and hollow BEC research is taking place at the moment. Based on the heritage of QUANTUS, MAIUS, and CAL, the Bose–Einstein condensate and Cold Atom Laboratory (BECCAL) is the follow-up facility under development for experiments on quantum optics, atom optics, and atom interferometry. It will also exploit the unique microgravity environment of the ISS[28] and provide laser cooled ensembles and BECs of Rb and K, along with various options for trapping and manipulation, for studying fundamental physics and advancing quantum sensors. BECCAL is expected to enable experiments on coherent atom optics, scalar and spinor BECs, quantum gas mixtures, strongly interacting gases and molecules, as well as quantum information. Its capabilities will include single- and dual-species atom interferometers, allowing tests of concepts and developments for future space-borne quantum sensors in dedicated missions.

In China, the CACES mission and Chinese space station are developed under the support of the China Manned Space Program (CMSP). The Cold Atom Clock Experiment in Space (CACES) project kicked off in 2011 with the goal of operating a rubidium microwave clock in space. It was launched in September 2016 with the Chinese space laboratory Tiangong-2 and put into operation for over 15 months in orbit as reported in 2018. Moreover, the science module II of the Chinese space station is due to launch in 2022 with a Cold Atom Physics Rack (CAPR), whose aim is to achieve picokelvin expansion energy levels and explore the physics of quantum magnetism, exotic material, acoustic black holes, and the Efimov effect.

3. Missions scenarios and studies

Many of the aforementioned initiatives were triggered by the PHARAO/ACES[6] and the HYPER[7] proposals back in the beginning of the 21st century. Since then, many more advanced proposals have been issued, addressing fundamental aspects such as investigating future gravitation and general relativity related theories, exploring dark matter and dark energy, observing gravitational waves, or measuring the earth geoid with unprecedented accuracy. Table I summarizes the major projects submitted and considered in the last two decades by the community.

Two major routes, using similar technological design for quantum sensors, have been extensively studied in the last decade: testing

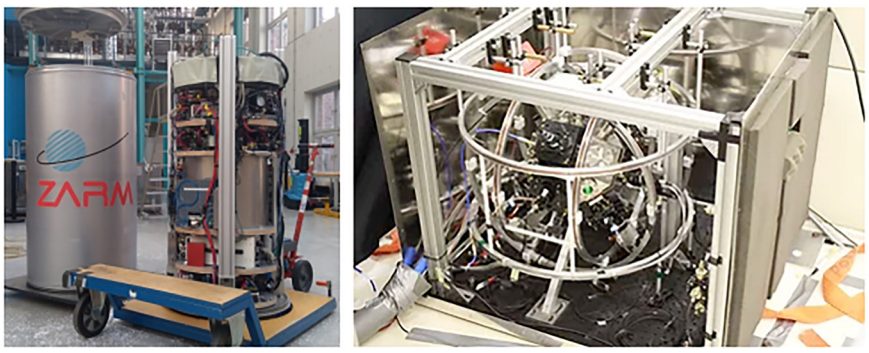

FIG. 3. The QUANTUS (left) and ICE (right) experiments performed in the frame of CNES, DLR, and ESA initiatives.

TABLE I. List of proposed cold-atom based missions currently under study or operation.

Mission	Target	Performance goal	Status	References
STE-QUEST	UFF test	$\eta = 10^{-15}$–10^{-17}	Voyage2050 proposal	29
AEDGE	GWD and DM search	GWD in the 10^{-2}– few Hz, ultralight DM fields	Voyage2050 proposal	30
SAGE	Multi-purpose gravity explorer mission		ESA's call "new ideas" 2016	31
AIGSO	Gravitational-wave (GW) space observatory	Middle-frequency (0.1–10 Hz) GW detection	In progress	32
SAI	Transportable atom interferometer	High-flux atomic source	ESA pre-phase—a study	24
CAI	Gravity field recovery	Sensitivity of 5 mE/$Hz^{1/2}$	ESA ITT study	33–35
CAL	ISS multi-user facility	Cold atom physics, atom interferometry	NASA mission—in progress	10
BECCAL	ISS multi-user facility	Cold atom physics, atom interferometry	DLR-NASA mission—payload development in progress	28
CAPR	Cold atom physics, atom interferometry	Chinese space station	In progress	36
GRICE and CARIOQA	Gravity field recovery	Gradient sensitivity of 10^{-14} s^{-2} $Hz^{-1/2}$	CNES phase-0 study and EU program	18
MAIUS-2/-3	Explorer for dual species atom interferometry in space	Quantum mixture physics, dual-species AI	DLR-mission—qualification in progress	9
HYBRID	Electrostatic-atomic accelerometer concept		ESA study	37

the universality of free-fall with a differential gravimeter using two different atomic species at the same location, and space geodesy using differential gravimetry with the same species at two different locations.

a. Fundamental physics in space: The equivalence principle. Einstein's Equivalence Principle (EEP), which is a cornerstone of general relativity (GR), postulates that the inertial mass and gravitational mass of any object are equal. This assumption implies that, in the same gravitational field, two bodies of different masses or compositions will undergo the same acceleration. This sub-principle of the EEP is known as Weak Equivalence Principle (WEP), or as the Universality of Free Fall (UFF). Various theories of quantum gravity predict a violation of the EEP,[38,39] hence detecting the presence or absence of a violation at a very high precision would help to put bounds on these theories. The central parameter that characterizes the WEP is called the Eötvös parameter η, which is defined as the ratio of the differential acceleration between two bodies to their mean acceleration $\eta = 2\frac{|a_1 - a_2|}{|a_1 + a_2|}$, where a_1 and a_2 are the gravitational accelerations of test bodies 1 and 2, respectively. This parameter evaluates to zero if the WEP is respected.

Today, the most precise tests of the WEP have been carried out with "classical" test masses (i.e., masses made of bulk material) at the level of 10^{-13} via torsion pendulum[40] or lunar laser ranging[41] experiments. Recently, the MICROSCOPE space mission[42] has been launched and demonstrated a measurement of η at 10^{-14}. Benefiting from the low background noise and permanent free fall of an orbiting satellite, it is expected to reach a demonstrated test at 10^{-15}. In contrast, the majority of WEP tests using cold atoms have been carried out on ground, in well-controlled laboratory environments, and have not yet reached a level of precision competitive with those done with classical bodies. Nevertheless, tests using "quantum" bodies like atoms are sensitive to WEP violations resulting from quantum physics that cannot be otherwise accessed. Presently, the state-of-the-art[43] for this type of measurement has reached long-term sensitivity and accuracy of $\sim 5 \times 10^{-11}$, while most experiments reached low 10^{-8} accuracy and sensitivity using cold samples of ^{85}Rb and ^{87}Rb,[44,45] or ^{87}Rb in mixtures of different internal states.[46] Lower sensitivity was demonstrated when using different atomic species.[47,48] So far, two main approaches have been taken to improve the sensitivity: (i) atoms launched in a fountain to extend their free-fall time inside large-scale vacuum systems[17,49] or (ii) atoms contained within a small-scale apparatus that is then placed in free fall, such as in a drop tower,[15] a sounding rocket,[50,51] or an aircraft undergoing parabolic flight.[8]

ESA studied different routes to test the universality of free fall with quantum sensors in space. The Space-Time Explorer and QUantum Equivalence Principle Space Test (STE-QUEST) mission was a phase A study following the pre-selection of cosmic vision medium size mission.[25] In parallel, ESA funded the Quantum WEP (QWEP) study to explore possibility to carry out such test on the ISS, targeting 10^{-14} accuracy.[16] As for all other missions proposals, it was based on the simultaneous measurement of the free-fall acceleration of two different atomic species, or isotopes, by an atom interferometer. By using the same atom optics tools to manipulate, the wave-packet of the two atomic species, such an experiment can achieve an extraordinary level of common-mode acceleration noise suppression, especially if two isotopes of the same atom are used. The test masses considered were two free falling ensembles of ^{85}Rb and ^{87}Rb cold atoms. The two ensembles were prepared and interrogated simultaneously, and the differential acceleration was measured. The selected location was

within the Columbus module, in an International Standard Payload Rack (ISPR). The dimensions of the Physics Package were compatible with the internal volume provided by an ISPR four-post configuration. The environment (Columbus, ISS, Earth) was analyzed, and disturbing effects were assessed. According to the error analysis, a WEP test by atom interferometry with 10^{-14} accuracy objective appeared feasible, in about 2 years of shot noise-limited measurements in the microgravity environment offered by the ISS.

b. Space geodesy: Cold atom gradiometer in space. Satellite earth observations enable the monitoring of mass and mass transport in the Earth system and provide a significant contribution for understanding the Earth and monitoring its changes related to geodynamics and climate change.[52] Some initial concept studies on the impact of cold atom technology for space geodesy were performed in the frame of the GRICE assessment study realized by CNES. Different instrument configurations and mission scenarios were reviewed, and a preliminary performance analysis of a promising candidate was realized.[18,53] The configuration was of a GRACE-like long baseline gradiometer, based on a constellation of two satellites, flying at an altitude of 370 km. Each satellite embarks a cold atom accelerometer with sensitivity (for an interrogation time $2T = 1$ s) of 6×10^{-10} m/s^2. $\tau^{-1/2}$ (τ is the averaging measurement time). Both satellites are connected by a laser link that would measure the inter-satellite distance. Simulations showed best performance in terms of monthly gravity fields recovery under 1000 km resolution, with improvement on the order of 10% to 25% over the traditional range-rate approach in the 222–1000 km resolution bands. In parallel, a detailed design and performance analysis of a 3D Cold Atom Interferometer (CAI) gradiometer for space geodesy, based on the concept proposed by Ref. 33, was studied in Refs. 34 and 35. With an instrument sensitivity of 5 mE/Hz$^{1/2}$ (where $1E = 10^{-9}$ s^{-2}) and a mission at an altitude of 239 km, the gravity field recovery was shown to get improved by a factor 2 for spherical harmonics degrees above 50 for the expansion of Earth's gravity field, and significantly better for lower orders, when comparing an 8-month model obtained with the CAI gradiometer with the model obtained from GOCE data over its whole duration.

A specific concept of inertial sensor based on a hybrid atomic-electrostatic accelerometer has also been studied.[37] This concept relies, on one hand, on the electrostatic technology developed for many years for the different space geodesy missions CHAMP, GOCE, GRACE, and GRACE-FO.[20] It offers a high level of performance in terms of acceleration sensitivity and naturally a high degree of maturity. On the other hand, the hybrid concept is also based on the emerging cold atom technology that seems very promising in this context. Each of these two types of instruments has its own assets which are, for the electrostatic sensors, the demonstrated short-term sensitivity, continuous nature of the measurements, and high TRL, and for CAI, among others, the absolute nature of the measurement and, therefore, no need for calibration processes. These two technologies seem in some aspects very complementary, and a hybrid sensor bringing together all their assets could be the opportunity to take a big step in this context of gravity space missions. Note that similar hybrid schemes based on cold atoms coupled to seismometers or force balanced accelerometers have been studied extensively.[54] They have led to the development of state-of-the-art cold atom gravimeters. The hybrid scheme has also been a key element for the success of onboard inertial measurement demonstrations in a boat[55] or in an aircraft.[8,22] This concept has been naturally extended to space applications and its potential studied in Ref. 37 for GRACE-type and Bender-type satellites configurations. These simulations showed that improved gravity retrieval could be achieved for some level of low frequency atomic instrument performance. The hybrid instrument allowing also a better knowledge of the scale factor accelerometer has shown that the drag-free requirements on the satellites could be relaxed.

All these efforts lead the agencies, such as NASA, to include atom potential gravity mission (MCDO) in their decadal survey[56] or the EU to include the development of a quantum space geodesy payload prototype.[57]

II. SPACE ATOM INTERFEROMETRY

Sven Abend, Baptiste Allard, Aidan S. Arnold, Ticijana Ban, Liam Barry, Baptiste Battelier, Ahmad Bawamia, Quentin Beaufils, Simon Bernon, Andrea Bertoldi, Alexis Bonnin, Philippe Bouyer, Alexandre Bresson, Oliver S. Burrow, Benjamin Canuel, Bruno Desruelle, Giannis Drougakis, René Forsberg, Naceur Gaaloul, Alexandre Gauguet, Matthias Gersemann, Paul F. Griffin, Hendrik Heine, Victoria A. Henderson, Waldemar Herr, Simon Kanthak, Markus Krutzik, Maike D. Lachmann, Roland Lammegger, Werner Magnes, Gaetano Mileti, Morgan W. Mitchell, Sergio Mottini, Dimitris Papazoglou, Franck Pereira dos Santos, Achim Peters, Ernst Rasel, Erling Riis, Christian Schubert, Stephan Tobias Seidel, Guglielmo M. Tino, Mathias Van Den Bossche, Wolf von Klitzing, Andreas Wicht, Marcin Witkowski, Nassim Zahzam, and Michał Zawada

A. Basic principles

Atom interferometers exploit the wave-like properties of matter. They allow the measurement of a physical quantity (e.g., acceleration, gravitation, rotation) by extracting the phase difference accumulated between two spatially separated quantum paths followed by the atoms. A common way to manipulate the atomic wavefunction is using laser light in an analog of the Mach–Zehnder optical interferometer (see Fig. 4), with laser standing waves acting as mirrors and beam splitters. Interference between the two paths at the recombining beam splitter leads to a difference in the detection probability in each of the two output channels that is a sinusoidal function of the accumulated phase difference $\Delta\phi$. The sensitivity of such an interferometer is proportional to the area enclosed by the two atomic trajectories. For instance, if the platform containing the laser standing waves accelerates, or if the atoms are subject to a gravitational acceleration, the phase shift is $\Delta\phi = \boldsymbol{k}_{\text{eff}} \cdot \boldsymbol{g}T^2$, where $\boldsymbol{k}_{\text{eff}}$ is the effective wavevector of the Raman process, and $\boldsymbol{g}$ is the platform or gravitational acceleration. Compared to optical interferometers, matter-wave interferometers have the advantage to allow a longer interrogation times T, and the area can also be enhanced by increasing $\boldsymbol{k}_{\text{eff}}$;[58] the drawback is typically an increased selectivity on the atomic velocity, with an associated reduction of the number of particles effectively interrogated.

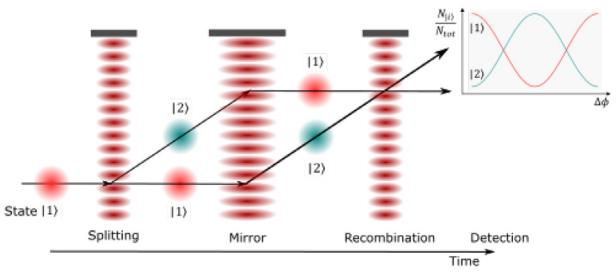

FIG. 4. The Mach–Zehnder configuration uses a series of three pulses: the first pulse separates the atomic wave, the second redirects the two partial waves, and the final pulse causes the two wavepackets to recombine and interfere. The interference is detected, for example, by measuring the number of atoms in one of the output states.

In a standard CAI, a sequence consisting of atom preparation, interferometer, and state detection is repeated with a period ranging from a few hundreds of milliseconds to a few seconds, allowing quasi-continuous measurement of the desired physical quantity. In the preparation stage, atoms are laser cooled to a cloud that can be subsequently cooled by evaporation to reach ultracold temperature. The free falling cold atom cloud then undergoes a sequence of coherent state splitting, exchange, and recombination using Raman or Bragg transitions driven by a phase controlled lasers pair. Finally, the output atomic quantum state is measured using fluorescence or absorption imaging.

AIs can perform very accurate and sensitive measurements such as, for instance, the effect of electric or magnetic fields on atoms, the mass of an atom (for tests of certain fundamental laws of physics), decoherence and collision effects (index of refraction for atomic waves), and inertial effects such as the acceleration of gravity (with possible applications in mineral prospecting) or the rotation/acceleration (the AI then becomes an inertial sensor).

The first demonstrations of measuring accelerations[59] and rotations[60] with atom interferometers occurred in 1991. Recent work has demonstrated that rotations and accelerations can be monitored with extremely high accuracy and sensitivity.[13] Following developments have extended their range of applications to fundamental physics, industrial use, and metrology. They were used in a Kibble balance that serves as the redefinition of the kilogram.[61] A pair of spatially separated interferometers interrogated by the same laser can be used to measure the gravity gradient with rejection of common mode noise sources such as vibrations. Such gravity gradiometers can measure the gravity gradient of the Earth[62] as well as the gravity gradient associated with nearby mass distributions. They achieved resolutions below 1 E and were used to measure the gravitational constant G.[63–66] In addition, the same technology can be used for gravitational wave detection.[67–69]

B. Alternative AI geometries

Other configurations are possible depending on the specific sensitivity required to different inertial effects. Four and five pulses configurations are considered for gravitational waves detection and allows to cancel rotation issues, acceleration noise, and gravity gradient background.[70] Interleaved measurements[71] are also considered when the interrogation time (typically of order of 10 s in a space mission) can be longer than the cycling time (typically of order of 1 s). It, thus, requires launching the atoms, to separate the region where the atoms are produced and the one where they are interrogated. This adds complexity and brings a first-order sensitivity to rotation, due to the non-zero average velocity of the atoms.[35]

Multi-axis measurements are also possible and they bring clear added value in the fields of geophysics, navigation, and accelerometry. A sequential strategy can be achieved by switching the light between the different axes. Moreover, simultaneous measurements can be achieved using multi-axis atom optics theoretically studied in Ref. 72. Associated to double diffraction (see Sec. III E and Fig. 11), it is possible to get all the information in one shot with a linear combination of the phases and obtain both rotation and acceleration signal. An alternative approach uses two differential Mach–Zehnder interferometers from the single source with sequential orthogonal operations,[73] see Fig. 5. It measure one axis of rotation and one axis of acceleration at the same time and discriminates between them with a scheme similar to Ref. 74. In consequence, a fully six-axis measurement is obtained using three experimental runs of different orientation.

C. Specific needs for space

Because their sensitivity scales with the interrogation time $2T$ (and even the square of $2T$ for inertial sensing), AIs can largely benefit from the long free fall time in space. For that, many challenges have to

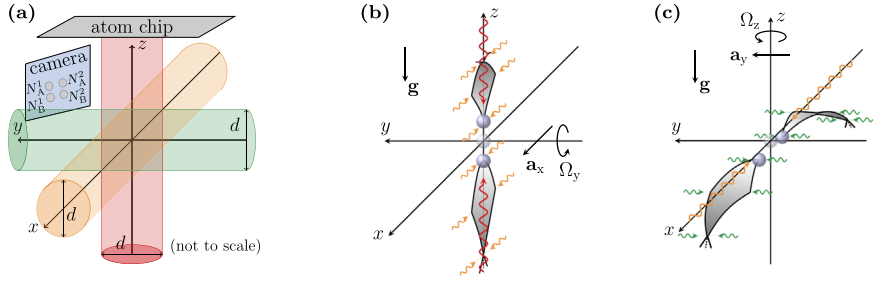

FIG. 5. Reprinted with permission from Gersemann *et al.*, Eur. Phys. J. D 74, 203 (2020).[73] Copyright 2020 Authors, licensed under a Creative Commons License. Setup to measure all components of $\vec{\Omega}$ and $\vec{a}$. (a) Three perpendicular oriented optical lattices in red (z-axis), green (y-axis), and orange (x-axis) are needed for the various diffraction processes. In order to measure $\vec{\Omega}_y$ and $\vec{\Omega}_z$, as well as $\vec{a}_x$ and $\vec{a}_y$, the direction of the double Bragg process to generate two initial wave packets is changed along the z-axis (b) or the x-axis (c). The corresponding interferometers are formed by three successive light pulses inducing double diffraction along the x- and y-axis, respectively.

be tackled. They relate not only to the general constraints imposed by space missions but also to specific aspects of the operation principle of the AI: the matter-wave manipulation process is significantly different from ground operations, the specificity of the space environment puts additional operational constraints, and the temperature of the atomic cloud impacts in several ways the sensor architecture and its performance.

1. Matter-wave beam splitters

The standard two photon diffraction process (e.g., Raman diffraction) uses retro-reflected interferometer beams in order to guarantee their relative phase stability and accuracy. On ground, this gives the possibility to select between two opposite diffraction directions, depending on the Doppler effect. In the absence of gravity, both pairs of interferometer lasers are simultaneously resonant, which leads to the so-called double diffraction scheme.[75] This latter method, as well as its generalization to Bragg diffraction,[76,77] requires that the atoms have a sub-recoil velocity distribution to be able to separate the different diffraction orders and allow for optimal operation.

2. Control of the environment

The sensitivity of the interferometer to rotations imposes constraints on the satellite attitude control that depend on the atomic temperature. This becomes more and more demanding when increasing the interrogation time, and eventually impossible to fulfill when operating Nadir. As an example, for an orbiting frequency of the order of 1 mrad/s, and an interrogation time of 10 s, a temperature in the femtokelvin range would be required to prevent a complete loss of contrast due to the averaging of Sagnac phase across the velocity distribution, when measuring the acceleration in the orbital plane. This effect can be in principle suppressed, if not efficiently mitigated, by counter-rotating the interrogation beams of the interferometer,[35] relaxing the constraints in the attitude control system, at the price of a demanding stability of the angular control of the laser system.

3. Temperature limit of interrogation time

The targeted long interrogation times of order of a few seconds result in an extremely low temperature required for the atomic sample to restrict the ballistic expansion of the atomic source. The use of standard laser-cooled atom sources even at their lowest temperature requires impractically large field of view for the detection system, considering that the size of a few μK cloud can be of the order of hundred millimeters after 10 s of interrogation time.

BEC samples combined with matter-wave lensing or delta kick collimation[78–81] offer a mitigation to all the above-mentioned constraints. They allow to reach subrecoil velocity distributions in the 10–100 pK range.[49] At such temperatures, the ballistic expansion is reduced by about two orders of magnitude with respect to laser cooling, allowing for double diffraction operation as well as long interrogation times. This also reduces the requirements on the attitude of the satellite is at the level of μrad/s in terms of control of residual rotations, which is within reach with current technologies, even at the lowest orbits.[82]

4. Ground based microgravity facilities

A fair extrapolation of the interferometer performances to interrogation times well beyond what can be reached on the ground is also needed. The interrogation times on earth are usually limited to a fraction of a second by the size of the vacuum chamber (up to about 2 s in 10 m tall facilities[83]). The difficulty of assessing the validity of instrument models, both in terms of measurement stability and control of systematic effects, makes tests in microgravity ground infrastructures of uttermost importance.

5. Test of systems and sub-systems in relevant environment

As any other space-borne device, all components have to be space-compatible, i.e., they must survive the launch and be able to operate under the conditions on board a satellite. This requires dedicated qualification tests, at the component, subsystems (in particular for the laser system and the vacuum chamber), and system level. It also demands significant engineering efforts to minimize the size, weight, and power budget, to make it fit with the possibilities offered by the targeted platform (being ideally a dedicated satellite) and to keep the cost of the mission affordable.

D. Space-borne atom interferometry applications

Bringing the interrogation time to tens of seconds will lead to single-shot acceleration sensitivities in the 10^{-12} m/s^2 range, competitive, if not better, than the best classical accelerometers designed for space operation, namely, the electrostatic accelerometers of the GOCE mission. Combined with the absence of drifts, this opens interesting perspectives for applications in the field of space geodesy and fundamental physics.

1. Space geodesy

Key performances of CAIs, namely, their sensitivity and long-term stability, would allow gravity missions embarking quantum accelerometers on dedicated satellites to improve spatial models of the geoid in a GOCE-like gradiometer mission configuration[35,52] and our knowledge of mass transport processes at low and medium degrees in a GRACE-like mission,[18,53] where accelerometers measure very precisely the non-conservative forces applied to the satellites.

2. Tests of general relativity

a. Weak equivalence principle test. Although very successful so far, GR as well as numerous other alternatives or more general theories of gravitation are classical theories, thus, fundamentally incomplete. Future space tests of the UFF, and more generally the EEP, are one of our best candidates for a major discovery that will revolutionize fundamental physics and our understanding in general of the laws of the universe at all scales including dark energy and cold dark matter. Europe has a clear lead in this field, through unique recent missions like MICROSCOPE[42] and LISA Pathfinder[84,85] and upcoming missions like ACES.[86] Mature mission concepts that can achieve uncertainties up to the 10^{-17} level in tracking a possible UFF violation were proposed.[29]

b. Lorentz symmetry and CPT violations. Lorentz symmetry is central to our current models of Quantum-Field theory. It is one of the pillars of the EEP. A violation of local Lorentz symmetry would alter our understanding of fundamental interactions and gravity. CPT-symmetry is also fundamental to all existing theories. A violation of CPT-symmetry would manifest itself in unequal moduli for the g-factors of the proton and anti-proton. Lorentz- and CPT-violating terms of the non-minimal standard model extension can also be constrained by searches for asymmetries in the dark-matter interactions of protons and anti-protons. Probing gravity with an atom interferometer can provide constraints on post-Newtonian local Lorentz invariance.[87] Enhanced gravitational wave detection can also lead to putting new limits on Lorents/CPT symetry.[88]

3. Gravitational waves and dark sector physics

a. Gravitational waves detection. Establishing a network of gravitational wave observatories opens the path toward novel tools in astronomy enabling the observation of previously undetectable phenomena. Ground-based laser interferometer detectors, such as advanced VIRGO, advanced LIGO, GEO-600, and others are designed to detect relatively weak, transient sources of gravitational waves, such as coalescing black holes, supernovae, and pulsars in the frequency range of tens of Hz up to a few kHz. Signals at frequencies below 10 Hz are masked on Earth by seismic and Newtonian noise when using state-of-the-art optical interferometers. This limitation motivated the drive for space missions such as LISA Pathfinder[84,85] and LISA[89] to perform millihertz gravitational wave detection circumventing ground limits. Ground-based AIs are indeed ultimately limited at frequencies approaching a fraction of a Hz and space-borne detectors are, therefore, vital to probe the lowest frequencies.

b. Dark matter, dark energy searches. Dark matter (DM) and dark energy (DE) are the main contributions to the average energy density of the universe. Their precise nature remains, however, elusive despite decades of advances in astrophysics and high-energy physics experiments. Atom interferometry in space could be an important complementary technique to explore certain theories involving chameleon- or symmetron-field models.[90,91] In these theories, light scalar fields mediate long-range interactions that could be detected by AIs which have already excluded part of the parameter space for these models.[92–94] Further constraining these models requires, however, longer interferometry times only possible in a space environment.

4. Quantum physics

a. Quantum superposition principle and decoherence tests. The superposition principle, stating that a quantum system is able to simultaneously occupy more than one quantum state, is central to quantum mechanics. Its applicability to macroscopic systems is, however, problematic as experienced in everyday life. Models of decoherence, caused by the entanglement of physical systems to the environment, could be tested to assess the applicability range of the superposition principle.[95] Interferometric and non-interferometric tests of models of spontaneous wave function collapse[96] could be deployed to probe the loss of quantum coherence of systems as they become more massive or if observed for long times (seconds) as could be offered in a space-borne experiment.[97]

b. Quantum gases physics. Quantum many-body research has had a tremendous boost since the production of ultracold matter and more specifically the realization of Bose–Einstein condensates and degenerate Fermi gases. A very active field concerns the validation of strongly correlated bosons and fermions theories, thanks to the high level of control in cold atom systems. Indeed, one could emulate a large variety of effects across several fields, such as quantum chromodynamics (QCD), astrophysics, and high-energy physics. Earth gravity is a major perturbation of the atomic systems making the space operation of freely evolving cold matter an ideal environment to pursue many-body physics quests.

Addressing these ambitious objectives constitutes a long-term goal of the atom interferometry community in Europe. Preparatory actions have to be undertaken from now on, to increase the level of maturity and the space adequacy of the involved technologies, and it is an objective of this paper to review their status and identify the needed scientific and R&D activities to be pursued in future. In addition to this long-term strategy, it is important to take advantage of any opportunity that may open on the path, such as a pathfinder mission aiming at technology demonstration on a dedicated platform or as a host on an existing platform, such as the ISS for instance.

III. ATOM INTERFEROMETERS: KEY COMPONENTS AND THEIR DEVELOPMENT PLANS

Sven Abend, Baptiste Allard, Aidan S. Arnold, Ticijana Ban, Liam Barry, Baptiste Battelier, Ahmad Bawamia, Quentin Beaufils, Simon Bernon, Andrea Bertoldi, Alexis Bonnin, Philippe Bouyer, Alexandre Bresson, Oliver S. Burrow, Benjamin Canuel, Bruno Desruelle, Giannis Drougakis, René Forsberg, Naceur Gaaloul, Alexandre Gauguet, Matthias Gersemann, Paul F. Griffin, Hendrik Heine, Victoria A. Henderson, Waldemar Herr, Simon Kanthak, Markus Krutzik, Maike D. Lachmann, Roland Lammegger, Werner Magnes, Gaetano Mileti, Morgan W. Mitchell, Sergio Mottini, Dimitris Papazoglou, Franck Pereira dos Santos, Achim Peters, Ernst Rasel, Erling Riis, Christian Schubert, Stephan Tobias Seidel, Guglielmo M. Tino, Mathias Van Den Bossche, Wolf von Klitzing, Andreas Wicht, Marcin Witkowski, Nassim Zahzam, and Michał Zawada

In this section, we describe the main subsystems of a CAI, more specifically in the context of space applications. Figure 6 presents the diagram including all the key components required to build a CAI. The atoms are isolated from the environment inside a high-vacuum chamber (Sec. III A). In the first stage of the experiment, the atoms are cooled and trapped in a specific configuration of crossed laser beams (Sec. III C) generated by a cooling laser system (Sec. III B) and forming a 3D magneto-optical trap (MOT). Then, a second stage of cooling and trapping is necessary to further reduce the velocity dispersion of the atom source and control accurately the position of the center of mass; such stage can be implemented, for example, by an optical

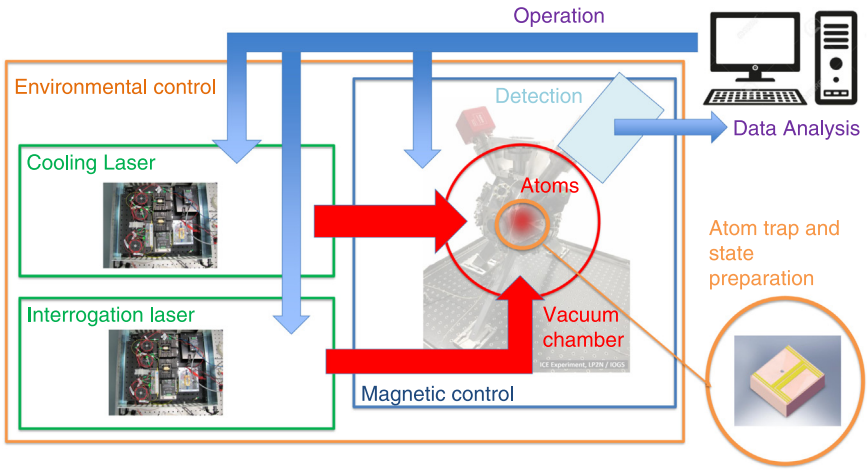

FIG. 6. Diagram showing the key components of a cold atom interferometer. The atoms are confined and isolated from background collisions in a vacuum chamber. They are cooled and trapped by a first laser system (cooling laser) before a second stage of cooling, trapping, and preparation phase to put them in the good quantum state (atom preparation). For the inertial measurement they are then manipulated by a sequence of pulses supplied by a second laser system (interrogation laser). A detection system allows the measurement of the atomic phase which is then processed to extract the relevant signal (data analysis). A shield and a series of coils are required to control the magnetic environment around the atom cloud (magnetic control). The environmental control includes the management of parameters, such as rotation, gravity gradient, and non-inertial acceleration.

dipole trap or an atom chip. The atoms are then prepared in a well-defined quantum state (Sec. III D). The third phase of the sequence consists in applying a series of light pulses to achieve an atom interferometer sensitive to the targeted inertial effect (e.g., acceleration, rotations, gravity gradient). These multi-photon transitions are operated with a second laser system with specific requirements (Sec. III E). The population ratio at the output of the CAI is then detected (Sec. III F). The atomic signal is then processed by a data analysis adapted to the applications (Sec. III G). All the experimental sequence is included in a magnetically controlled environment using magnetic shields and coils pairs (Sec. III H). Last but not least, the specific environment onboard a satellite, in terms of rotations, gravity gradients, or spurious vibrations, has a strong impact on the operation of the CAI and needs to be taken into account. We present the different approaches to tackle these constraints (Sec. III J). Recent implementation of atom interferometry in microgravity or in space[9,10,26] made the demonstration of a relatively high level of TRL for the different technologies involved, and in particular for the atomic source[98,99] and the laser systems based on semiconductor lasers and discrete optics[100] or on fibered telecom lasers.[101,102]

A. Vacuum system

1. State-of-the-art

Cold and ultracold atom experiments need to be performed under high-vacuum (HV) or ultrahigh vacuum (UHV) conditions, respectively, to reduce collisions with background particles. Therefore, the atoms are prepared and manipulated in actively pumped vacuum chambers.

Different approaches exist to set up such vacuum vessels. A straightforward way is to assemble the vacuum vessels using standard ConFlat (CF) steel parts. These systems are easy to assemble and maintain, but are typically heavy and bulky and lack small viewports with good optical quality. Additionally, the magnetic properties of steel (even 316LN) is not favorable for ultrahigh precision experiments using ultracold atom technology. To improve on the magnetic part, aluminum chambers have widely been used. These chambers are easy to be milled in desired configurations, but typically prevent the use of the CF sealing technique due to the softness of the material. To still be able to attach viewports or vacuum pumps, sealing techniques using indium or lead wires have been established. Thanks to the indium sealing technique, arbitrary small viewports with best optical quality can be employed. Due to the progress in milling machines and tools over the past years, titanium chambers are often used nowadays in high demanding ultracold atom experiments. They allow for CF connections as well as indium or lead sealing and show very beneficial magnetic properties. A totally different approach to the use of metal is the use of glass vacuum chambers. These chambers typically feature very good optical access with good optical quality and can be quite compact. The drawback of this approach lies in the use of a quite fragile material and a strongly reduced freedom in the design of the system, since these glass chambers typically feature only one port to attach vacuum components. Additionally, the necessary peripherals, like coils or collimators, cannot be rigidly attached to the glass chambers, but need an additional frame, which typically increases the size of these systems again significantly.

To establish the HV or UHV conditions in these systems, the vacuum is initialized using external roughing pump systems to reach the necessary low pressure to switch on the HV or UHV pumps of typically better than 10^{-8} mbar. After this point, the roughing pump system can be detached utilizing bulky vacuum valves or single-use copper pinch of tubes and the built-in HV or UHV pumps maintain the vacuum. Here, typically a combination of an ion getter pump (IGP) and a titanium sublimation (TSP) pump or a non-evaporable getter (NEG) pump is used. IGPs are typically heavy, bulky and rely on strong magnetic fields, which demands a careful placement of the

pump with respect to the high-precision measurement zone. TSP pumps operate via the evaporation of pure titanium from filaments, which can demand high currents of more than 20 A. NEG pumps can show release of dust particles when put under vibrational loads.

2. Development plan

The vacuum system sits at the heart of the entire apparatus (Fig. 7 shows the vacuum system of MAIUS-A). Its size sets the bounds for the outer lying components such as the diameter of the electromagnetic coils or an overall surrounding magnetic shield. In total, this is a large factor in the mass budget of the full apparatus, and its scale-down is, hence, of critical importance. Therefore, the development is focused on the miniaturization of the vacuum system.

For purely MOT operating systems, progress has been reported[103,104] on miniaturized vacuum systems with pressures in the 10^{-7} mbar regime. This is enough for MOT operations but too high for ultracold atoms where a pressure in the 10^{-11} mbar range is required. UHV conditions are typically reached by using additional getter pumps such as TSP or NEG. The improvement of these pumps is, therefore, of high priority. Improved getter materials may reduce the size requirements on the ion pump or—ideally—replace it completely, as it has been demonstrated for a limited time in.[103,105]

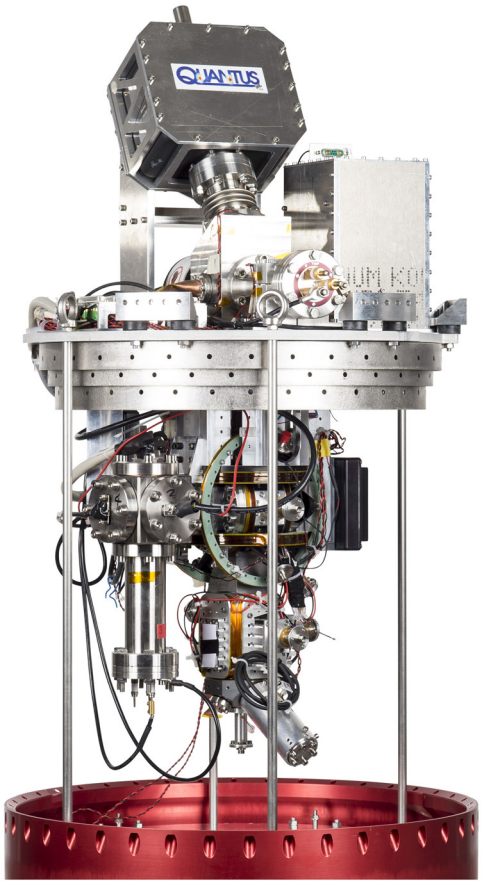

FIG. 7. The vacuum system of the sounding rocket payload MAIUS-A.

This would not only remove mass and power demands but also avoid stray magnetic fields inherent to ion pumps. If the ion pump cannot be fully dismissed, the magnetic stray fields will strongly influence the atomic ensembles in a close miniaturized vacuum system due to the proximity. It may, thus, be necessary to operate the ion pump not from permanent but from electro-magnets. In this way, the vacuum pumping and atomic system would be operated in an interleaved fashion.

The construction of the main vacuum chamber requires a careful choice of materials. For example, the permeation of helium through different glass materials can be vastly different[106] and, thus, put additional demands on the vacuum pumps which should be kept at a minimum. Furthermore, outgassing properties need to be taken into account where especially titanium and aluminum show excellent performance[107] and also have favorable magnetic properties. The use of novel construction techniques, such as additive manufacturing, may open up additional miniaturization opportunities. However, these need to be developed for the respective materials and surface qualities in order to minimize the possible outgassing area. Advanced pumping concepts may also seal these surfaces with getter materials that act as a large-area passive getter pump.

B. Laser architecture for cooling

1. State-of-the-art

Recent implementation of atom interferometry on board a sounding rocket[9,108] demonstrates the high TRL for the different technologies involved, and in particular for the atomic source[99] and the laser systems based on semiconductor lasers and discrete optics.[100,109] Currently, further miniaturization and space qualification is done.[28] Alternative laser technology based on fibered telecom lasers are also planned for experiments, for which prototyping activities[101,102] and space qualification are underway. In both architectures, the electronics required for the laser system includes low noise current sources, temperature stabilization devices, and frequency and phase locks to control the optical properties of the laser source and the active components (modulators, shutters) of the beam distribution system. Typically, low current noise is provided with long-term drifts below the μA level and the temperatures of the laser diodes are stabilized at the level of 1–10 mK. The required frequency stability of the laser source is typically $\approx$ 100 kHz.

a. Semiconductor lasers. Semiconductor diode lasers have long been the foundations of cold atom experiments in the laboratory. Their compact size, relatively low electric power requirements, and low cost make them prime technologies for space missions.[51,110,111] In particular, the high-tunability and narrow linewidths of Extended Cavity Diode Lasers (ECDLs), Distributed Bragg reflector lasers (DBRs), and distributed feedback lasers (DFBs) make them especially popular for laser cooling and atom interferometry. Diode lasers typically require amplification to reach the optical powers required for such applications. This is frequently achieved by pairing the laser with a semiconductor optical amplifier [Ridge-waveguide Amplifier (RWA), or Tapered Amplifier (TA)] in a discrete architecture with a seed of several $\sim$ W amplified to the order of 1 W;[10,112] however, such systems usually come with a large footprint and larger sensitivity to changes of the environment such as vibrations and temperature. A

compact alternative is to use a microintegrated, master oscillator power amplifier (MOPA) arrangement in which a semiconductor laser such as an ECDL is microintegrated alongside an amplifier chip as operated in sounding rockets in recent years.[9,51,110,111] Such laser types offer of the order 500 mW in output power.[109,113,114] High beam qualities of single-mode diode lasers and emission in the multiple W range, as used in optical dipole traps, may be achieved with tapered lasers.[115]

b. Telecom lasers. Telecom lasers are robust solutions for future space missions. Using second harmonic generation to generate near infrared light (767–780 nm), this technology applies for rubidium and potassium. Many of these fiber-coupled sources are already Telcordia qualified, satisfying demanding specifications in terms of vibrations, shocks, temperature variations, and lifetime. Moreover, these commercial products constitute a large catalogue of highly reliable and/or redundant components. This includes narrow linewidth laser diodes suitable for atom interferometry, phase/intensity electro-optical modulators (EOM) to simplify architectures and to provide fast tunability, acousto-optic modulators (AOMs), Erbium Doped Fiber Amplifier (EDFA), and fast photodiodes. Radiation hardness has also been tested for a number of these components and a few of them are now space qualified. The most sensitive component is the EDFA but specific doped fibers have been developed to tackle this issue. The frequency doubling stage is a robust pigtailed periodically poled lithium niobate (PPLN) waveguide, providing high efficiency and delivering high optical power at the output of a mono-mode optical fiber (typically 500 mW). Telecom lasers are present in the first commercial atom gravimeters,[116] experiments in microgravity,[117] compact navigation devices,[118] and atomic based gravitational waves antennas.[102]

c. Distribution/modulation. Another critical issue is the laser conditioning and distribution. Ais have very stringent requirements with respect to spectral purity and to intensity stability and control. For example, the MOT stage requires hundreds of milli-Watts of power, whereas even the scattering of a few resonant photons can cause a deterioration of the interferometry signal at later stages of the experimental sequence. Undesired side-bands in the frequency spectrum of the lasers can cause similar problems, e.g., shifts in the fringes and loss of contrast. These characteristics cannot be met with current all-in-fiber laser conditioning systems, thus necessitating a distribution/conditioning breadboard. In contrast, free-space optical systems with fiber in and out coupling offer a robust and efficient solution which can be seeded by a variety of lasers and used in combination with some fibered components (e.g., AOMs and beam splitter). Various approaches to these free space systems have been taken including the metal breadboards,[100,112] 3D printed modular cube systems,[119] high mechanical and thermal stability Zerodur based benches,[120,121] micro-integrated ceramic benches,[122] or commercially available fiber port clusters.[123] Ultrastable breadboards have been developed in the context of two ESA projects, achieving a stability of the coupling efficiency of better than 1% rms fluctuations even under 8 g acceleration and 40 K temperature cycling.[124,125] Such systems receive light from the master-laser and amplifier; condition it using optics such as beam splitters, dichroic mirrors, polarization optics, AOMs/EOMs, mechanical shutters; and finally couple the light back into optical fibers. Suitable shutter and RF-drivers are commercially available as well as

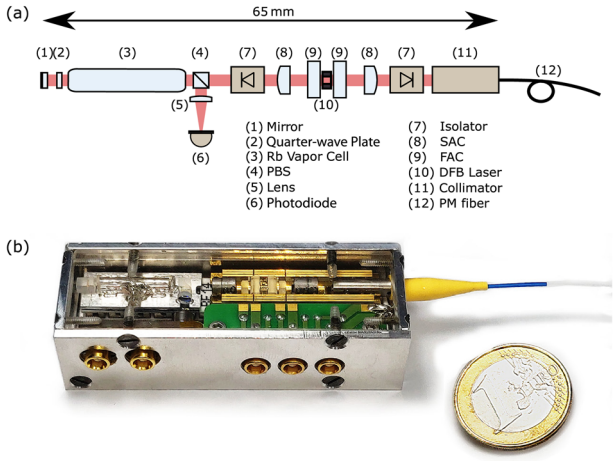

FIG. 8. The design (a) and a photo (b) of a compact optical frequency reference for Rb as described in Ref. 129.

photodiodes to monitor laser light levels and to generate beat notes for frequency stabilization.

Another approach to simplify the distribution/modulation is to reduce the number of lasers required by employing additional frequency modulation techniques. For example, setups have been realized that use a single diode laser to perform all the operations of the AI,[126] exploiting, for instance, carrier suppressed, multiple single-sideband modulated laser sources[127] or dynamical offset locks of single lasers used for laser cooling.[128] In addition, functional units can be integrated such as the laser light source and spectroscopy unit[129] as shown in Fig. 8.

These solutions, in addition to fiber coupled AOM and EOMs (at near visible and telecom wavelengths) for frequency modulation, shifting and pulse shaping, fibered cavities for spectral cleaning of unwanted sidebands, fiber switches for light switching and shutting, and fiber beam splitters for overlapping can lead to more compact and simplified optical bench setups.

2. Development plan

This section summarizes the current efforts in developing more mature and compact laser systems for atom cooling and trapping.

A space qualified fibered laser system is currently developed.[130] Microintegrated diode lasers have already flown in various missions; however, further, more complex missions are in various stages of development. For example, the MAIUS-1 payload[9,100] has been further developed into the MAIUS-2 payload which is due to fly in a sounding rocket in 2022/23. Further to this, the BECCAL mission is due to launch to the ISS in 2026,[28] the BECCAL laser system provides the light fields required for a wide variety of ultracold atom-based experiments, including dual-species interferometry with rubidium and potassium atoms.

To further reduce the size, weight, and power (SwaP) of optical distribution modules, miniaturized modulators (AOM, EOM), optical shutters together with discrete optics need to be microintegrated and qualified for space application.

Ultimately, photonic integration of the laser source[131] including the development of optical components which can be integrated in

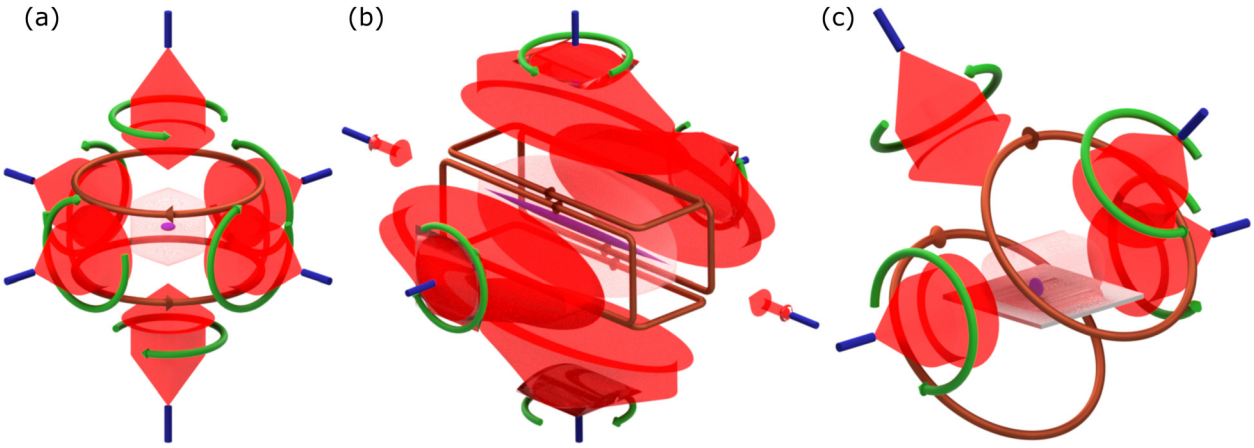

FIG. 9. Magneto-optical trap geometries: six-beam 3D MOT (a), a 2D(+) MOT (b), and reflection 3D MOT (c). The blue fibers deliver cooling and repumping light (red) which is collimated by lenses and appropriately circularly polarized (green arrows) with quarter-wave plates. Beam overlap regions are in light red, with MOT shape in purple. The vacuum pump, cell, and atom source are omitted for clarity, but anti-Helmholtz magnetic coils and current flow are indicated (copper).

photonic circuits will lead to photonic chips offering the needed functionality.

C. Magneto-optical traps

1. State-of-the-art

The "workhorse" for most cold atom experiments is the six-beam MOT [Fig. 9(a)]. Atoms collect at the center of a 3D magnetic quadrupole field beam, from the overlap volume of three (orthogonal) pairs of appropriately circularly polarized red-detuned counter-propagating laser beams.[133] Cooling and trapping hinge on radiation pressure variation due to the Doppler and Zeeman effects, respectively. In a relatively pure vapor of the species of interest, the maximum MOT atom number is independent of pressure, but the maximum is reached at a rate proportional to pressure. Differentially pumped systems use a "high" pressure atomic vapor in conjunction with, e.g., a 2D MOT [Fig. 9(b)] or Zeeman slower to load either a "low" pressure 3D MOT [Fig. 9(a)], or alternatively a reflection MOT [Fig. 9(c)] to aid compatibility with chip trapping, albeit with half the effective beam overlap volume and an off-axis magnetic quadrupole.

In most laser cooling experiments, whether loaded by a slowed beam or directly from the vapor, the main figure of merit is the beam intensity. Loading and cooling mechanisms begin to saturate in terms of flux or atom number when the beam intensity is comparable to the stretched-state beam intensity I_S on the main cooling line, moreover the laser linewidth should ideally be less than the atomic linewidth (Table II). Laser beam quality for cold atom loading is quite forgiving; however, reaching the lowest sub-Doppler temperatures requires radiation pressure intensity balance in each dimension at the atom location below around 10%,[134] with residual magnetic bias fields $\ll 1$ G.[134,135]

2. Development plan

Cold atom experiments typically require large experimental apparatuses. There have been major advances in the lasers, electronics, vacuum cells, and atom chips culminating in space systems;[9,10,137] however, optical beam delivery is still a key restriction on valuable payload volume. For all portable applications, single-input beam MOTs offer a valuable alternative, with options including pyramidal and grating MOTs (Fig. 10), with compact applications also foreseen in navigation, exploration, telecommunications, metrology, and medical imaging.

Standard pyramid MOTs [Fig. 10(a)[138–140] and variants[141,142]], tetrahedral pyramid MOTs [Fig. 10(b)],[143] and grating MOTs [GMOTs, Figs. 10(c)–10I][144,145] make all but one of the standard MOT beams redundant. The advantages of the other geometries over the standard pyramid are *ex vacuo* optic operation, non-critical geometry, and the removal of beam shadowing in large MOTs. Large samples are possible, $\sim 10^8$ ^{87}Rb atoms from a 2×2 cm^2 grating, with single-cell vapor MOT atom number scaling as $d^{3.6}$ for beam diameter d, the same as a standard MOT.[145] Phase-space density has been optimized,[146] and sub-Doppler cooling of millions of atoms down to 3 μK in a GMOT is also possible Ref. 135.

The grating optical design has been thoroughly investigated,[147,148] showing a remarkable wavelength versatility—a single grating could in principle trap all atomic alkali metals. GMOTs have already found applications in magnetometry,[135] atomic microwave clocks,[149] accurate high vacuum pressure measurement,[150] and ultracold electron beams.[151,152] The GMOT has also demonstrated compatibility with the latest advances in miniaturized vacuum chamber

TABLE II. Key laser trapping and cooling parameters: the wavelength λ, the transition linewidth Γ, the stretched-state saturation intensity $I_S = hc\pi^2\Gamma\lambda^{-3}/15$,[136] and the axial MOT magnetic field gradient B_1.

Atom	Li	Na	K	Rb	Cs	Sr	Yb	Sr_n	Yb_n
λ (nm)	671	589	767	780	852	461	399	689	556
Γ (MHz)	5.9	9.8	6.0	6.1	5.2	32	31	0.007	0.183
I_S (mW/cm^2)	2.6	6.3	1.7	1.7	1.1	43	63	0.003	0.139
B_1 (G/cm)	10	20	10	10	10	60	60	0.02	0.4

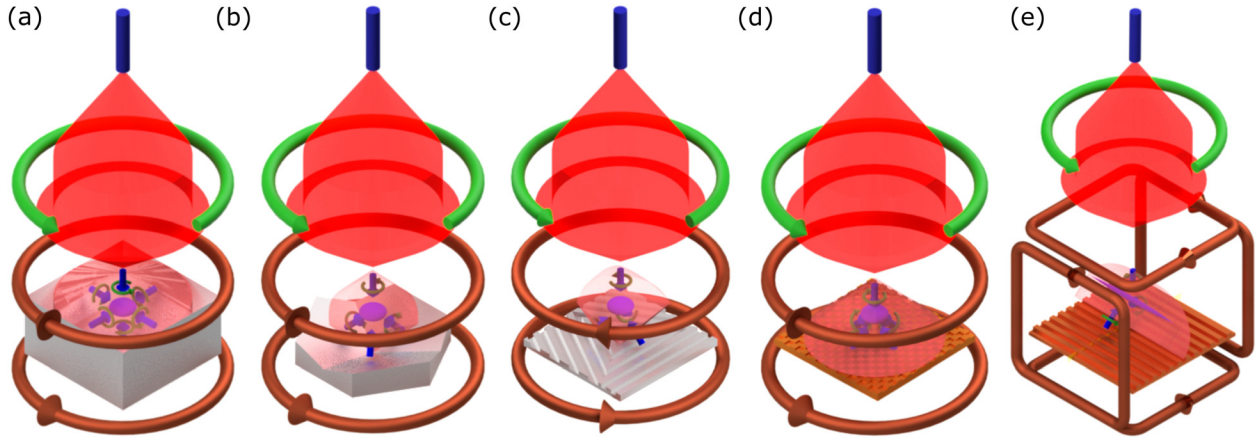

FIG. 10. Compact single-input-beam magneto-optical trap geometries, with Fig. 9 color scheme: pyramid MOT (a), tetra-pyramid MOT (b), 3D "triangle" grating MOT (c), 3D "checkerboard" grating MOT (d), and 2D grating MOT (e) as described in Ref. 132. In all geometries except (a) some of the beam overlap is above the pyramid/grating optic, which can be used *ex vacuo*. The vacuum pump, cell, and atom source are omitted for clarity.

technology,[103] magnetic chip traps,[153] and grating holes can be used for Zeeman-slowed loading beams[154] or absorption imaging.[155]

In the most promising applications of time metrology, optical clocks based on alkaline-earth atoms are major contenders. An alkaline-earth atom GMOT has recently been generated,[156] highlighting the technology's versatility. Phase stable 3D and 1D optical lattices with a single input beam are also possible[145] either using the same grating as the GMOT or via separate 1 mm^2 grating regions on the same chip in the same vacuum chamber. This allows testing of a variety of optical lattice geometries and dimensionality, with a view to accurate clocks and quantum simulation.

In addition to optically compact cooling and lattice architecture, there is growing interest in the use of next-generation optical architecture[157] for atomtronic circuits in terrestrial and space applications, in order to extend atomic interrogation time for sensing and metrology.[158]

D. Ultracold atoms and state preparation

1. State-of-the-art

Specifications of atomic sources have been studied in the context of various proposals for space missions as mentioned in Sec. I D 3. They rise to technical challenges such as creating an ultracold source with temperature <100 pK, and reaching a significant flux of 10^6 atoms in few seconds and eventually being capable of dual atomic species operation. Most of the ultracold atom sources are based on a laser cooling stage followed by an evaporative cooling stage. We present the generic solutions used in the laboratory, which have given convincing results in on-board experiments.

a. Evaporative cooling in an atom chip. Atom chips were developed to trap and manipulate atoms in strong magnetic potentials generated by microfabricated current carrying wires.[159] This approach allows for strongly confining traps with high potential gradients enabling efficient evaporative cooling of the ensemble in compact and robust setups, like QUANTUS-1.[15,160] Building upon this approach, multi-layer atom chip assemblies allow the efficient trapping of μK hot molasses-cooled ensembles and lead to the demonstration of high BEC-flux of 10^5 atoms in 1 s.[99] Based on this low power consuming, compact and robust type of BEC source, the first BEC in space[9] and first atom interferometer in space Ref. 108 have been demonstrated on the sounding rocket mission MAIUS-1. Furthermore, a matter-wave lens system to collimate the BEC to a residual internal kinetic energy of 38 pK in 3D has recently been demonstrated in the free-fall of the droptower Bremen using QUANTUS-2.[99] All these projects rapidly advanced the TRL of the atom chip based BEC sources.

Recent further developments focus on the increase in the atomic flux, the displacement of atoms from the chip's surface toward the interferometric interrogation zone,[161] and the implementation of versatile interferometry schemes on ground[162] and in microgravity. Furthermore, the possibility of combining magnetic and optical trapping[122] in the perspective of multi-species experiments[27,28] are under investigation. For an even further increase in compactness and robustness, new approaches to combine the atom chip technology with planar gratings are ongoing.[104]

b. Evaporative cooling in a dipole trap. Optical dipole traps are good candidates when optical access and control of the atom interaction through Feshbach resonances are critical. Historically, dipole traps were achieved with high optical powers, of tens if not hundreds of watts.[163] Improved schemes requiring lower optical powers need to be investigated.

Efficient loading in dipole traps is a critical issue, especially when limiting the laser power, as this restrains the trade-off between trap depth and capture volume. A technique combining gray molasses and painted potentials has demonstrated a good loading efficiency in a compact system[98] and evaporation duration of the order of the second to reach BEC. First demonstrations of evaporative cooling in dipole traps in microgravity have been recently achieved. The ICE experiment installed in the 0 g simulator in Bordeaux is able to produce BECs in a dipole trap[98] and evaporative cooling during the microgravity phase has been demonstrated in the Drop Tower.[164] Dipole trap laser are also suitable for atom lensing, and 2D optical delta kick collimation has been demonstrated to reach a temperature of 50 pK.[49]

c. State preparation. Atom interferometers require atoms prepared in a single and long-lived internal state, usually a first-order magnetically insensitive sublevel of the hyperfine manifold $|F, m_F = 0\rangle$ for alkali atoms. In the case of BEC sources, the preparation step must not involve spontaneous scattering of photons, which would result in an excessive atomic heating. In an atom chip, the atoms are optically pumped beforehand in the state with the highest available value for m_F for which the magnetic forces are the strongest. Coherent multi-photon rf-transitions are then used to transfer atoms to $|F, m_F = 0\rangle$. In principle, in an optical dipole, trap all Zeeman states are equally trapped. With additional B-field gradient, it is possible to control the trap depth for states sensitive to magnetic fields. Therefore, during the process of evaporation, one can preferentially remove the latter states. At the end of the cooling process, it is possible to obtain a source of atoms prepared in a single Zeeman state. The spin-distillation method has to be characterized in a 0 g environment.

2. Development plan

To date, the best reported BEC-flux is of a few 10^5 atoms/s.[99,165] Proposals for future missions anticipate a BEC-flux of 10^6 atoms/s and more to reach the desired performance targets.[29,33] Atom chip technology offers rapid BEC production;[99] optimization of chip structures and transfer efficiency into the magnetic trap may increase the flux but require further investigation. For optical dipole traps, painted potentials can speed up the cycle rate[166,167] and are investigated for microgravity operation.[98]

a. Optimization of all optical atomic sources. Complex strategies, based on motorized moving lenses and additional optical lattices,[168] allow the production of large atom fluxes (up to 10^6 atoms in 3.6 s) but such solutions are currently not mature for space, and are inherently requiring high-power. Improving the electro-optical efficiency of the laser source is necessary to make this strategy compliant with a space mission.

Advanced laser cooling methods in dipole traps is appealing because the process can be very fast (∼100 ms) which mitigates atom losses. Raman cooling have been used to produced BECs but with a moderate atom number.[169] Alternatively, laser cooling in optical trap, combining the creation of dark states and a spatial modulation of the laser trapping the atoms,[98,170] needs to be investigated further to exploit its full potential. Atom lensing (3D delta kick cooling) is feasible especially with painted potentials to reduce the velocity dispersion. Continuous atom sources of rubidium using the transparency of the atoms related to the strong light shifts induced by telecom lasers can have an interest to increase the atomic flux.[171]

A dedicated development for the laser source is required, targeting a power reduction of the system and considering the specific requirements of the adopted cooling protocol as well as space qualification.[172]

b. Upgrade of atom chip-based sources. The advancement of atom chips targets multiple sub-components of the chip assembly. Typically, the multi-layer chip assembly consists of multiple lithographically structured wafers and a large thermal heat sink in which additional wires for the initial magnetic trap and the MOT magnetic fields are embedded. All components are glued together using a vacuum-compatible adhesive that has a reduced—but non-null—outgassing rate. Finally, the very top layer is provided with a dielectric mirror surface with a glued transfer coating. In this way, the glue acts not only as the joining element but also as a heat conductor and height-leveler between the layers. The advantage of this technique is the straightforward assembly process, but it comes at the cost of vacuum quality due to outgassing: the number of background particles is locally increased, which impairs the lifetime of the magnetic trap and, thus, the evaporation efficiency and finally the number of atoms in the BEC. It is, thus, a key objective to replace all adhesives in the assembly with other conjunction techniques with lower or no outgassing. A promising alternative technique is the transient liquid phase diffusion bonding, which relies on a metal-to-metal diffusion process that joins metalized surfaces without chemical adhesives. This technique solves the joining between the layers but is not applicable for the optical mirror coating. Here, a planarized chip surface is required to be able to coat the wafer with a dielectric mirror coating directly. Consequently, the wires must be manufactured within the wafer instead of being grown on top of it. The added advantage is that this also opens the possibility to use diffractive optical surfaces such as reflection gratings as the final chip layer. In this way, the single-beam BEC atom chip comes into reach where only a single optical beam is required to capture the atoms in the MOT phase and then the BEC is created in the magnetic trap. This has the potential to drastically shrink down the overall apparatus because far less optical access is required.

Intrinsically, the atom chip produces heat due to ohmic heating when current is sent through the wires. Since there is no air in the system that transfers heat through convection, it must be moved out through the atom chip assembly itself by conduction. Commonly, copper is used as the mounting structure for the wafers due to its high heat conductivity and low cost. However, the presence of bulk metal close to the chip wires impairs the switching characteristics of the chip wires due to eddy currents. These could be partially suppressed by elaborate placement of slits but never fully avoided. An alternative approach is to use special ceramics that have a high thermal conductivity but are electrically non-conducting. This will increase the amount of experimental control to the system by shortening switching times and ultimately lead to better performance in all parts that require precise switching of magnetic fields.[173]

E. Atom interferometry: Lasers, optics and atom optics

1. State-of-the-art

a. Atomic beam splitters and mirrors. In an atom interferometer, the coherent spatial separation of the wave packets is realized by atom–light interactions during a laser pulse. In most cases, two photon Raman transitions are used and Rabi oscillations between two (external and in some cases internal) states generate an atom beam splitter (for a quarter of an oscillation: $\pi/2$ pulse) or a mirror (for half an oscillation: π pulse). It is, for instance, possible to realize a Mach–Zehnder AI with a three pulses sequence $\pi/2 - \pi - \pi/2$. This type of interferometer is then sensitive to the spatiotemporal area defined by the two-photon recoil $\hbar k_{\text{eff}}$ and the interrogation time between two pulses T, both being very well controlled. This method guarantees the stability of the scale factor. Moreover, two counter-propagating beams are used to create a significant splitting of the wavepackets. The classical configuration for such Raman Ais is to

send the two required frequencies ν_1 and ν_2 in the same beam, which is then retroreflected onto a reference mirror. This mirror is in practice essential to define physically a phase reference for the inertial measurement. Consequently, two Raman transitions are possible: k_1 incident and k_2 reflected, or k_2 incident and k_1 reflected, k_i being the wave vector for the I frequency. In the case of a gravimeter, the degeneracy of the two Raman transitions is lifted thanks to the Doppler effect. Each Raman transition can be chosen by the sign of the frequency chirp applied to the frequency difference between the Raman lasers in order to compensate the Doppler effect and keep the Raman transition on resonance during the fall of the atoms.

In microgravity, as the Doppler effect is null, these two Raman transitions happens simultaneously. Depending on the atom temperature, the Raman Rabi frequency, and the choice of the Raman frequency difference, two regimes are possible: double single diffraction and double diffraction. The principle of the double single diffraction (DSD)[26] is to realize a velocity selection with the Raman pulses to a non-null value, "cutting" in the velocity distribution [see Fig. 11(b)]. Two symmetric velocity classes $\pm v$ are selected and each velocity class realizes an independent atom interferometer, the two interferometers having areas with opposite signs and opposite wave vectors $k_{\text{eff}} = k_1 + k_2$. Since each atom participates to only one of the two interferometers, we sum the probability transitions (and not the amplitude) corresponding to the outputs of each atom interferometer. The phase shift of the double single diffraction is then given by the following equation:

$$P = P_0 - 2A\cos\left(k_{\text{eff}} a T^2 + \delta\phi_{dep}\right)\cos\left(\delta\phi_{las} + \delta\phi_{ind}\right), \quad (1)$$

where a is the acceleration along the wave vector k_{eff}, A is related to the contrast of each independent interferometer, and $\delta\phi_{las}$ is the laser phase. $\delta\phi_{dep}$ and $\delta\phi_{ind}$ are contribution to the interferometer phase, which are dependent or independent of the direction of the wavevector k_{eff}. Notably, scanning the laser phase does not allow for scanning the interferometer fringe pattern and, thus, for measuring the inertial quantity of interest.

The double diffraction (DD)[75] regime consists in using a four-photon process involving atoms in the velocity class $v = 0$. Here, a single interferometer is realized with an area twice larger than the single diffraction interferometer [Fig. 11(c)]. The phase shift becomes:

$$P = P_0 - A\cos\left(2k_{\text{eff}} a T^2 + \delta\phi_{dep}\right). \quad (2)$$

The main advantages of the double diffraction are its sensitivity, which is doubled, and the reduced impact of systematics because of the symmetry of the interferometer, which adopts wavepackets in the same internal state along the two paths.

In both regimes DSD and DD, it is not possible to scan the interferometer phase with the laser phase difference, which results rather unpractical. Some applications do not require such control, for instance, differential measurements, e.g., WEP tests between two species or measurement of the gravity gradient. In the case of a single accelerometer, though, the motion of the mirror with respect to the atoms due to non-gravitational forces induces a phase shift, which corresponds to the signal of interest. The result is that the interferometer phase can be changed in a controlled way by shifting the position of this mirror.

Bragg diffraction is an alternative method for creating beam splitters and mirrors, based on the interaction of the atoms with 1D optical lattices. Similar to Raman transitions, it relates to the exchange of momentum between the atoms and counter-propagating lasers. A major difference with Raman transitions is that the atoms remain in the same internal state all along the interferometric sequence, so that a spatially resolved detection method is required. The advantage of Bragg transitions lies in the possibility to increase the splitting using multiphoton transitions, which boosts the scale factor and, thus, the sensitivity of the measurement. Bragg diffraction also allows the realization of the double diffraction protocol, which has similar features as in the Raman case.[77] Moreover, accelerating such optical lattices allows for atom launching via Bloch oscillations, and for increasing the

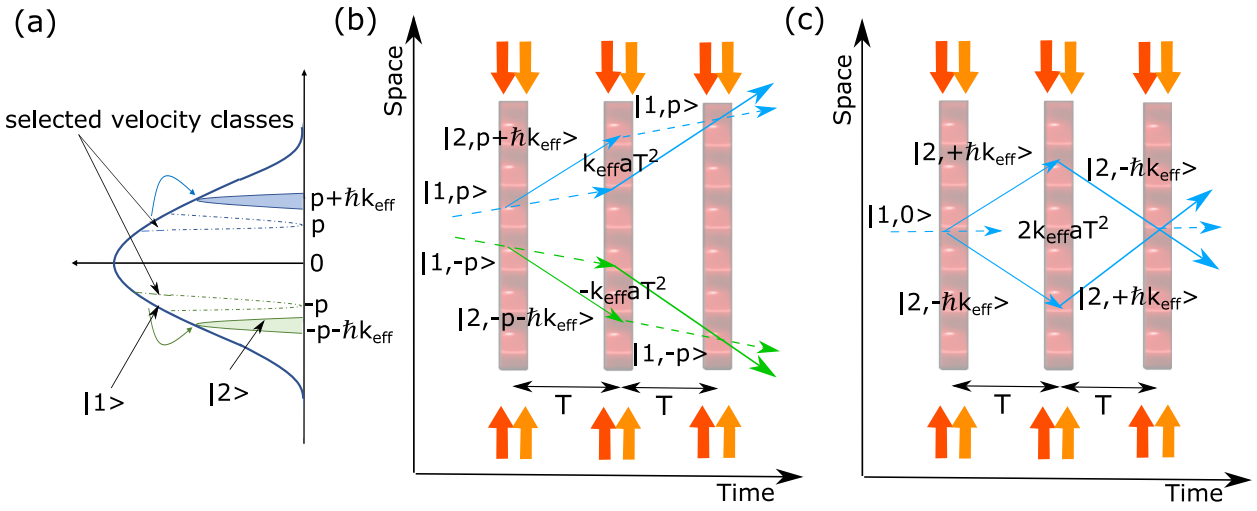

Fig. 11. Principles of the double single diffraction (a) and (b) and double diffraction (c) interferometer. (a) Velocity distribution of the atoms in microgravity. The Raman frequency is tuned near the half-maximum, simultaneously selecting two symmetric velocity classes $\pm v = \pm p/M$. (b) Double single diffraction interferometer trajectories. (c) Atom interferometer in the double diffraction regime as described in Ref. 75.

separation between the two arms of the interferometers by selectively accelerating and decelerating one or both arms. Bloch oscillations have been considered to separate an initial atom source into two clouds for performing gradiometric measurements.[35,174] Up to today, the largest internal momentum separations in atom interferometers have been exploiting optical lattices, thus allowing for large space time or real areas in short times.[175]

b. Requirements for the laser source. The technology is the same as for atom cooling with additional constraints in terms of phase noise and control of the Raman beams frequencies. For long interrogation time (>1 s), phase noise is typically specified below a level of 100 dBc/Hz at 10 Hz offset frequency. Phase modulators can lead to a strong reduction of the laser system complexity and are the natural choice to control the laser phase, but this solution brings an undesirable atomic phase shift due to the presence of parasitic lines.[176] Phase-lock-loops between two laser sources (preferentially low noise sources such as ECDLs) are usually used to guarantee a low phase noise level. Additionally, other specifications are critical, such as the Polarization Extinction Ratio (PER) which can be improved with polarizing components (e.g., cubes and polarizing fibers), an accurate control of the Raman pulse shape, and the power stability. This is even more true for space where we target a challenging accuracy of 10^{-12} or better.

c. Interferometry laser beam quality requirements. The quality of the intensity and phase profile must be at the highest degree over the whole size of the atom cloud, which for long interrogations times can reach a few millimeters.

The inhomogeneity of the laser intensity profile leads to non-homogeneous Rabi frequencies which then determines the efficiency loss for the atomic beam splitters and mirrors. The intensity fluctuations of the interferometry laser beam causes fluctuations of the atomic momentum, and then a systematic error.[177] Obtaining large areas with homogeneous laser light requires large power or top-hat beams.[178]

Wavefront aberrations leads to a systematic phase shift which is very difficult to model since the knowledge of the wavefront profile need to be known. This is one of the major limitations for the technology on ground at the 10^{-10} level, and the increased performance sought in space (10^{-12} or better) increases our demand on the optics quality. On this topic, several solutions are currently implemented: the reference mirror can be installed inside the vacuum system to avoid the aberrations due to the view port; the laser beam can be corrected using adaptive optics;[179] the optical aberrations can be measured using ultracold atoms.[180]

2. Development plan

a. Atom interferometry. The demonstration of double diffraction in microgravity, the extension of the interrogation time, and the investigation of systematic errors are at the heart of the demonstration activities in μg facilities (Einstein Elevator, 0 g simulator in Bordeaux, ISS with CAL/BECCAL program) described in Sec. III K.

b. Raman/Bragg laser source. A new scheme of phase/intensity modulations have been demonstrated and characterized.[127] This development allows to reduce the SwaP budget of the laser source.

c. Laser beam quality. Improving the intensity profile of the top-hat beams is at heart of the spatial CAIs. Active optical components, such as spatial light modulators to shape the phase polarization and intensity profile are not mature and require further exploration. The wavefront quality of the reference mirror and the quarter wave plate requires a dedicated engineering and maybe a dedicated characterization bench since our requirements challenge the state-of-the-art.

F. Detection

1. State-of-the-art

The phase difference between the two paths of the interferometer is extracted by probing the final quantum state of the atoms after recombination. This is usually done by measuring the relative populations in the two eigenstates (internal electronic state for Raman interferometry, velocity, or position for Bragg interferometry), either by collecting a fluorescence signal on a photodiode or by imaging the atoms on a CCD camera. While the former is usually more simple and compact, the latter is usually preferred for ultracold atoms in microgravity as it allows to extract more information.[181]

In a sequential detection scheme,[182] populations in the two output ports are imaged one after the other by using different detection beams tuned to different detection frequencies or by successively detecting one state, repumping the other state to the first one and detecting again on the same transition. Sequential imaging is simple to realize but it is limited by atom loss to unwanted transitions, and is affected by laser frequency and intensity noise, requiring a dedicated stabilization.

Simultaneous detection[183] requires a spatial separation between the two output ports of the interferometer. When the atomic velocity spread is smaller than the velocity kick given by the beam splitter pulse, this is achieved by simply waiting for the two clouds to spatially separate after the recombination pulse. This method allows for continuously repumping loss channels, yielding a larger signal to noise ratio, and common mode rejection of laser frequency and intensity noise. On the other hand, it introduces a dead time in the sequence.

The use of a CCD camera for simultaneous detection allows to retrieve the atom spatial distribution, reducing the systematic errors introduced by a partial overlap of the two clouds and, thus, relaxing the requirement on spatial separation. It also gives the possibility to characterize velocity dependent phase shifts and measure the phase and contrast in a single shot via the application of a controlled phase shear along the cloud.[184]

Alternatively for Bragg interferometry, Raman spectroscopy allows momentum resolved detection which does not require spatial separation.[185]

2. Development plan

A spatially resolved detection system is usually preferred as it allows to extract additional information about the trajectory of the atoms that can be crucial for the study of systematic effects. A measurement of the cloud velocity, which cannot be retrieved from the interferometer phase, can be used, for example, to assess for a residual Coriolis rotation bias. In addition, in case of nadir pointing, the large constant rotation rate imposed to the system induces a centrifugal acceleration bias to the signal. A precise analysis of the atomic

trajectory during the interferometer will be needed to determine this bias. Ideally, two imaging systems along the directions orthogonal to the interferometer probing direction will provide three-dimensional imaging.

A detailed study of the detection subsystem will help determining the precise geometry as well as the CCD cameras requirements in terms of speed and pixel size. The choice of absorption or fluorescence imaging technique will be based on the interrogation time and temperature of the cloud. For the large interrogation time expected in space, fluorescence imaging should be preferred as the atom cloud is more dilute.

G. Data analysis

The output phase signal of the interferometer is extracted from the measurement of the population in the output ports of the interferometer. As for any two-wave interferometer, for which the fringe pattern is a cosine function of the phase, the measured phase is restricted to a π interval, leading to phase ambiguity. In practice, methods are used to extend the unambiguous phase interval[186] or to compensate the interferometer phase shift, by using ramps and/or jumps in the laser phase[187] or frequency,[188] or alignment,[35,189] bringing it ideally down to a null phase shift, free from ambiguity. In practice, a modulation is often applied to keep the interferometer operating at mid fringe, where its sensitivity is optimal. Uncontrolled parasitic phase shifts (such as, for instance, due to non-inertial linear accelerations, or to their imperfect determination with additional classical sensors, when hybridizing quantum and classical measurements[187]) and detection noise may lead to significant phase scatter, which must be kept in a limited range (of order of a few hundreds of mrad) for accurate phase determination. The use of phase shear detection methods discussed above alleviates this requirement, as it allows for the extraction of the interferometer phase with an uncertainty independent of its value. As for differential measurements, various differential phase extraction protocols have been demonstrated, such as, e.g., based on direct ellipse-fitting,[190] Bayesian statistics,[191] direct extraction,[192] use of more than two interferometers,[193] and frequency shift of the mirror pulse,[194–197] with in most cases similar insensitivity to the actual phases of the two interferometers. Recently, methods based on consecutive[198] or simultaneous[199] interferometers with slightly different scale factors were demonstrated, which suffers far less from phase ambiguity and improve by orders of magnitude the dynamic range of the measurement. This short review of methods shows that the interferometer data analysis for accurate phase determination strongly depends on the interferometer configuration and the detection method.

The details of the data analysis will depend, thus, on the mission operations scenario. Separating gravity signals from non-inertial linear accelerations and parasitic forces due to satellite rotations is a key task. Quite generally, specifying a relatively high level of satellite attitude control will simplify data analysis, which will also benefit from additional signals provided by attitude sensors (e.g., star trackers and gyroscopes, mirror rotation control system). Calibration phases could be necessary to evaluate a number of key parameters for this data analysis, such as, for instance, the position of the atoms with respect to the center of mass of the satellite or with respect to the mirror. Details on the data analysis plan lie beyond the scope of this paper.

H. Magnetic control of the environment

1. State-of-the-art

Magnetic stray fields can adversely affect the preparation of the atoms, the interferometric sequence, and other manipulations.

A low-noise stable magnetic field is crucial for a good performance of the atomic trap described in Sec. III D as well as for the operation of the interferometer. Noise arises from fluctuations in the DC magnetic field caused by magnetized parts in the immediate environment and external geomagnetic field. These magnetic fluctuations can be either actively, or passively compensated.

Passive compensation often relies on a shield that redirects magnetic fields to energetically favorable paths. This results in a significant reduction of the magnetic field inside it. The shield is built of mu-metal, a magnetically soft nickel–iron–alloy with very high relative permeability μ_r (10^4 to 10^5). Mu-metal is UHV compatible and suitable for shielding against low-frequency ($\sim$10 Hz depending on the thickness of the layer) or static magnetic fields. Mu-metal shielding properties may be substantially degraded when exposed to high magnetic fields of $\sim$1 T. In such situation, the permeability can be reduced even to nearly 1.

Apart from the permeability, the shielding performance depends also on the geometry of the mu-metal shield. The ideal shape of a magnetic shield is a sphere or an infinite cylinder. Sharp edges and openings in the shield lead to magnetic flux leakage weakening the shielding effect. Therefore, rounded and cylindrical shapes with a minimized number of openings and precise mechanical machining and welding are preferable. To improve shielding effectiveness, multi-layer mu-metal shields are usually implemented since the total screening factor of the magnetic field is proportional to the product of the screening factors for all layers individually. For the existing versions of multi-layer shielding solutions, the attenuation of the external magnetic field of the order of 10^7 is achievable.

Optimal shielding results from a compromise between spatial restrictions, reduced weight, minimized number of openings, and performance. Multi-layer shielding requires the radius of the layer to be doubled with every new layer, which leads to an increase in size and mass (mu-metal has a high density of 8.7 kg/m^2). This is unacceptable for space due to payload limitations. For the same reason, the layers have to be as small as possible. The CD magnetic field present, for instance, for the MOT can then result in a saturation of the mu-metal. Optimal solution can be found by simulating of the magnetic shielding for different geometrical configurations with computer aided design (CAD) supported by the finite-element method (FEM) 3D numerical simulations.

The current design for quantum sensors usually uses shields outside the vacuum chamber.[9,28,108,200,201] These shields feature one[74] or multiple layers[9,28,108,200,201] and are usually cylindrical,[9,108,200] cubical,[10,28] or octagonal[201] with feedthroughs for cables, optical fibers, and other connectors. Although the shield itself is passive, additional coils can be required for the operation. The actual implementation is trade-off between available budget, sensor size/shape, required feedthroughs, and targeted performance. Reported shielding factors range from 18 for a compact setup[200] to 4000 (in certain directions) at 0.01 Hz for large devics.[201] Magnetic shields are currently used on the space missions (CAL[10] and MAIUS[9,108]), but their performance do not allow for high-sensitivity atom interferometry the alternative to

magnetic shields requires magnetometer measurements, compensation coils, and active feedback control.[202,203] The advantage of this active compensation is its compactness and the possibility of reducing inhomogeneous or time-dependent magnetic fields. The three-axis magnetic sensor has to be placed as close as possible from the center of the interferometer area. Instantaneous feedback to the PID controllers drives the current of three pairs of independent compensation coils. This allows the compensation of DC and AC magnetic fields. However, due to its high level of complexity, which entails non negligible risk of failure, active shielding is not the preferable solution for space missions.

2. Development plan

Magnetic shielding is essential in designing ultracold atom-based systems, requiring either a highly controlled magnetic environment or at least minimum stray magnetic fields. Currently, the best available materials for passive magnetic shielding are soft magnetic alloys consisting of nickel, iron, copper, molybdenum, and small amounts of various other elements, such as silicon or chromium. Such materials have high relative permeability values of 10^5. Depending on the composition, such materials differ in the ease of shaping. They are usually formed into the sheets needed for multi-layer magnetic shieldings.

Although mu-metal shielding is widely used, its high weight and manufacturing limitations make it unsuitable for space-oriented projects. Shielding materials are manufactured in simple geometries, which are known to provide reliable parameters. Moreover, to give a reliable shielding, the end product is characterized by a relatively high thickness which significantly increases its weight.

To overcome this limitations, new technological need to be developed. One of the promising emerging technologies capable of dealing with these issues is additive manufacturing, such as 3D printing, in which the shielding structure is built layer by layer. This approach enables complex while lightweight magnetic shielding geometries. Utilizing a high-power laser to melt powdered mu-metal locally allows customization of the alloy composition. The first results of this technique have been reported[204] showing shielding factors within a factor of 3 of conventional approaches. Although beneficial in the creation of complex geometries, the method needs further advancements in terms of the reduction of porosity in the printed structure to improve shielding per unit weight factor.

I. Operation

1. State-of-the-art

The experimental setup encompasses a control system, which includes a computer associated with input/output modules providing all the analog and digital signals to automatically produce the experimental sequence, with a time resolution of 100 ns or better.[205] The system is connected to the physics package and the laser package to synchronize the operations of the experimental sequence, like controlling the laser frequencies and optical powers, switching the laser beams and the magnetic fields, and triggering the detection. Most of the time the same sequence is repeated continuously, including the most common experimental steps, i.e., laser cooling and trapping, preparation in the good quantum state, interferometry pulses, detection. Data acquisition units are used to record the photodiodes and other monitoring signals. The control system is synchronized with a stable and accurate reference clock. Automatic locking electronics guarantee the robust functioning of the laser system.[206]

In terms of data management, the main measurements are the fluorescence signals collected by a photodetector, and series of spatial imaging of the atom clouds on the CCD camera for which the required resolution strongly depends on the purpose of the mission and can potentially be critical if not well assessed. In addition to the atomic signals, useful monitoring of external parameters are essential for diagnostic, for passive post-correction or active real time feedback. Examples of these parameters are the temperature of the critical components (laser source, and amplifier among others), the residual magnetic field in the physics package, the Raman laser power, and residual acceleration and rotations. Depending on the scientific objective, the data processing could include a lock-in algorithm or a Kalman filter[207] to track the atom fringes,[208] a differential phase extraction method in the case of a gradiometer,[209] or a double species interferometer for the WEP test.[210] Modulating the laser power and alternating the wave vector k_{eff} between shots allows to reject systematic errors mainly due to residual magnetic field or non-perfect interaction between the atom and the laser field (e.g., the intensity and phase inhomogeneity, and the light shifts). In addition, dedicated sequences of calibration can be realized to evaluate the residual bias once the latter rejection method is implemented.

2. Development plan

Space-borne operation implies limited rates for downstreaming data and limited remote access for uploading commands. Consequently, developments on onboard data evaluation, especially including images of the atoms, are desirable, both for downlinking pre-processed data, and for driving autonomous optimization (e.g., by differential evolution[211,212]) and self-calibration routines.

J. Environmental requirements

1. State-of-the-art

a. Non-inertial acceleration. For high precision tests of fundamental physics, residual acceleration of the reference mirror must be strongly reduced, similar to what has been demonstrated in space by LISA Pathfinder.[84] For geophysical missions where we want to distinguish the residual acceleration from the gravity field, hybridization with electrostatic accelerometers[37] can be considered. Other methods imply the use of differential accelerometers (gradiometers) allowing to reject a significant portion of the residual non-inertial acceleration noise.

b. Rotation compensation. Rotations have a strong influence on an AI, implying a loss of contrast and unwanted inertial terms leading to a bias of the measurement. The control of rotation of the satellite (AOCS) can be done combining space gyroscopes (e.g., iXblue Astrix) at short term and star trackers for long-term stability. Unfortunately, the performances are not good enough for most of the applications ($T > 1$ s, $\delta\Omega < 1\ \mu$rad/s). To solve this problem a tiptilt mount to rotate the reference mirror is considered. Piezoelectric technology is promising for the active "real-time" control of the Raman beam and allows to reach very high resolution (20 nrad). As an alternative, a

solution developed for LISA (PAAM: Point Ahead Angle Mechanism) can be adapted to our application.[89] This solution allows to rotate the mirror around an axis in the mirror plane. Such a system has been implemented on the ICE experiment and has been tested on an optical bench, including a position detector and an optical system to increase the sensitivity of the angle measurement. The precision of the compensation system is evaluated at 300 μrad/s for T = 1 s on the relative angle of the reference mirror between two pulses and needs to be improved by more than two orders of magnitude for future space missions.

Finally, the performances of the gyroscopes and the tiptilt mount need to be adapted to the high level of control required for a dedicated space mission. The state-of-the-art tiptilt mount in terms of resolution (20 nrad) is sufficient for most of the scenarios, but accuracy needs to be evaluated. A specific development to optimize the power consumption is also required.

c. Gravity gradient compensation. Similar to rotations, gravity gradients can lead to reduction of the contrast in an atom interferometer and induce systematic uncertainties.[25,213,214] Provided sufficient knowledge about the gravity gradient, appropriately adjusting the two-photon detuning of the beam splitting laser for the central pulse in a three-pulse geometry can compensate it for atom interferometers in a gradiometer or dual-species scheme for testing the universality of free fall.[194,196,215,216]

In the context of space missions, this approach was considered in a mission study for a gradiometer[35] and in the analysis of systematic errors for a test of the universality of free fall.[189] Since extended free evolution times beyond $2T = 2.6$ s are anticipated in these proposals, the lasers will need to have a larger accordability while still comply with the strict requirements in mass, power, and volume of a space borne platform. Additionally, a feed forward will be required to steer the detuning according to local changes of the gravity gradient.

For a single-axis accelerometer based on atom interferometry, the gravity-gradient compensation scheme is not applicable, since the main phase term canceled in a differential measurement remains. In this configuration, the residual expansion rate needs to be adjusted to retain contrast.[25]

2. Development plan

a. Rotation compensation. More specific studies are required, with tests targeting a good control of the rotation rate. A motorized rotative platform supporting the payload is required and will allow to optimize the lock-in electronics parameters. Moreover, this platform is required for the characterization of the gyroscopes and the tip-tilt mount.

The BECCAL project plans to operate three-pulse Ais with total free fall times of up to $2T = 2.6$ s onboard of the ISS. To maintain contrast, tip-tilt stage will be implemented featuring an appropriate dynamic range to compensate the rotation rate of about 1.1 mrad/s in nominal nadir pointing mode during the 2.6 s.

b. Gravity gradient compensation. While the concept for gravity gradient compensation was demonstrated in ground-based setups, qualification for a dedicated space mission remains to be shown. Especially when targeting free-fall times beyond a few seconds, a frequency comb or a high-finesse cavity to ensure frequency and phase stability of the detuned beam-splitting light field may be required.[189]

K. Microgravity testing platforms supporting the current and future development plans

Several platforms allow to perform relevant and complementary tests in microgravity, from ground-based installations (e.g., 0 g simulator in Bordeaux and Einstein elevator in Hannover) to space crafts (ISS, sounding rocket). In each case, there is a trade-off between convenience, duration of the microgravity phase and the level of residual accelerations and rotations. Usually, the test conditions are far from the quiet environment expected on a satellite supporting the foreseen scientific mission but are enough to tackle non negligible issues. We emphasize here the importance of performing atom interferometry in microgravity before the scientific mission. Double diffraction of the matter-wave packets[75] (or double single diffraction[26]) is the natural regime and needs to be studied in detail, and the absence of the gravity sag influences the production of the atom source. Moreover, microgravity allows to increase the interrogation time and, thus demonstrate the potential gain in sensitivity expected on the satellite. Finally, our models of the systematic errors, taking into account Raman beam imperfections, effective magnetic field, and gravity gradient among other, need to be validated experimentally. The platforms are presented here in the logical order considering the development of a future space instrument, starting from a barely consolidated sensor head compliant with the 0 g simulator in Bordeaux, going through different stages of development to reach a complete integrated and automatic system on a spacecraft.

1. 0 g Simulator in Bordeaux

The 0 g simulator installed in Bordeaux provides a fast and easy access to microgravity. The 3-m-high installation fits in a standard lab and produces 500 ms of microgravity every 13 s. The platform is compliant with significant payloads, tolerating a maximum weight of 250 kg and dimensions included in a cube of 1 m^3, without limitation in terms of power consumption. The movement of the platform is a vertical controlled parabola over a height of 70 cm with a residual acceleration noise of 5 mg and a residual rotation rate of 5 mrad/s. A recent demonstration of an all-optical BEC in microgravity[98] paves the way to future experiments using ultra cold gases, demanding a high repeatability and a good control of the parameters. The 0 g simulator is compatible with a large range of experiments previously mentioned, and it is useful to prepare parabolic flight campaigns on the plane or on the sounding rocket. Notably, the simulator allows to produce Moon or Mars gravity as well.

2. 0 g Plane

Parabolic flights onboard the 0 g plane give access to repeated parabolas with 20 s of microgravity. Historically, the first onboard AI[8] and the first WEP test using cold atoms in microgravity[26] have been achieved on this platform. The main limitations are the high level of residual accelerations (50 mg) and a high rotation rate (10 mrad/s). These issues are very difficult to tackle for atom interferometry with long interrogation times but are relevant to study the production of the atom source and increase the TRL of the different subsystems. The

0 g plane consists in a flying laboratory, with specific security rules for the mechanics, laser, and electronics. The payload does not need to be integrated; for instance, the ICE experiment includes ten racks, 1500 kg, for a power consumption of 2000 W. The ICE experiment is modular and flexible, allowing to test different subsystems, such as the fibered lasers, frequency combs, and micro-optics beam splitters.

3. Drop tower

The Bremen drop tower offers an unique environment currently providing one of the best microgravity conditions on Earth. This facility has been the first one exploited to study interferometry with Bose–Einstein condensates in extended free fall. The tower offers up to 9 s of microgravity time in an experimental run, which represents about the duration envisioned for a space-borne interferometer. Consequently, atom interferometry experiments striving for seconds of free fall are one focus of the tower research, which allows for about two experimental runs a day.

4. Einstein elevator

Only recently, the Einstein elevator in Hannover started its first flights.[217] In this facility a gondola is actively driven by a linear motor that compensates for air friction. Inside the gondola, the pressure is lowered to 10^{-2} mbar and an experimental carrier can be decoupled from the structure to perform a free falling vertical parabola flight after an initial acceleration. The Einstein elevator is constructed to offer 4 s of microgravity time with a residual acceleration in the range of 10^{-6} g, similar to the drop mode of the Bremen tower, but capable of up to 300 experimental runs a day.[218] It offers a large flexibility as it allows for experiments with a mass up to a tonne, a volume of roughly 18 m^3 as well as adjustable acceleration conditions between 0 and 5 g.

5. Sounding rocket

Sounding rocket missions provide a relatively cheap access to space and, hence, are favorable for feasibility studies in risky endeavors. Their microgravity times of a few minutes exceed by far the free-fall times reachable in towers and elevators. During the parabola flight above the Kármán line, the residual acceleration caused by air friction reduces depending on the flight height to a minimum of 10^{-6} g. Compared to other discussed platforms, this vehicle gives further constraints in mass, volume, and power consumption and requires additional robustness due to vibrational accelerations during launch and re-entry into the atmosphere. At the same time, the apparatus needs to operate autonomously because of limited access from ground.

The achievements of the first BEC in space[9] and the proof of its coherence using atom interferometry[108] improved strongly the TRL of the atomic source and the different subsystems. The unique platform is currently utilized to prepare space missions such as BECCAL.

Table III. Summary of the state-of-the-art.

Components	Performance	TRL	Status	References
Vacuum chamber	$P < 10^{-10}$ mbar	6	Functional. miniaturization is welcome to reduce the SWaP budget.	99
Laser for cooling and trapping	Optical power 100 mW at the atoms, polarization < -23 dB, frequency stability $\sigma_\nu = 10^{-10}$ at 1 s	6	Functional. Semiconductor approach validated on sounding rockets. EM for telecom lasers planned for 2023.	100, 112
Magneto-optical traps	10^9 Atoms loaded in 150 ms	6	Functional. miniaturization is welcome to reduce the SWaP budget.	99
Magnetic control	Residual magnetic field below 0.1–1 mG depending on the applications	6	Functional. Important contribution in the SWaP budget.	
Final atom preparation	10^6 Atom cloud produced in 1 s, temperature 10–100 pK, in the correct Zeeman state (usually $m_F = 0$)	4	Proof of concept fully demonstrated in the lab, partially demonstrated in microgravity.	9, 81, 99
Interrogation lasers	Optical power 10 mW at the atoms for Bragg interferometry	3	Inertial measurement with extended interrogation time demonstrated only with differential measurements.	108
Detection	Atomic shot noise limited detection for a BEC based atom interferometer	3–4	Demonstrated on thermal clouds, in a differential BEC interferometer.	54, 73
Data analysis	Automated/onboard data analysis, automated feedback for optimization	2–3	Differential evolution algorithm implemented to maximize the number of trapped atoms.	99, 211
Environment control and operation	Noninertial acceleration, rotations, and gravity gradients compensations	3–4	Gravity gradient compensation for a differential measurement, rotation compensation demonstrated on ground, vibration noise rejection demonstrated on ground and in microgravity.	8, 17, 54, 196

6. International Space Station

The ISS can be seen as middle ground between 0 g planes, droptowers, or sounding rockets with limited accessibility and satellite platforms. It offers persistent microgravity conditions while not being as restrictive as a satellite, thanks to the possibility of astronaut intervention. This enables extensive statistics and systematic evaluations beyond the scope of 0 g planes, droptowers, or sounding rockets, both beneficial for the development of quantum sensors and precision experiments. Currently, the Cold Atom Lab performs BEC experiments on board of the ISS.[10]

L. Summary of state-of-the-art

Table III presents the current status of development of cold atom interferometers for space.

IV. NEXT STEPS FOR a EUROPEAN LEAD SPACE MISSION WITH ATOM INTERFEROMETRY

Sven Abend, Baptiste Allard, Aidan S. Arnold, Ticijana Ban, Liam Barry, Baptiste Battelier, Ahmad Bawamia, Quentin Beaufils, Simon Bernon, Andrea Bertoldi, Alexis Bonnin, Philippe Bouyer, Alexandre Bresson, Oliver S. Burrow, Benjamin Canuel, Bruno Desruelle, Giannis Drougakis, René Forsberg, Naceur Gaaloul, Alexandre Gauguet, Matthias Gersemann, Paul F. Griffin, Hendrik Heine, Victoria A. Henderson, Waldemar Herr, Simon Kanthak, Markus Krutzik, Maike D. Lachmann, Roland Lammegger, Werner Magnes, Gaetano Mileti, Morgan W. Mitchell, Sergio Mottini, Dimitris Papazoglou, Franck Pereira dos Santos, Achim Peters, Ernst Rasel, Erling Riis, Christian Schubert, Stephan Tobias Seidel, Guglielmo M. Tino, Mathias Van Den Bossche, Wolf von Klitzing, Andreas Wicht, Marcin Witkowski, Nassim Zahzam, and Michał Zawada

Table IV presents the main developments planned in the next few years. At this stage, reducing the power budget is one of the major challenges for the cold atom technology. The most critical sub-systems are the laser amplifiers, and the RF active components, like, e.g., the AOM drivers and the magnetic fields to trap the atoms. Power management can be optimized by turning off the critical components when possible to reduce the average power consumption to this regard it must be remarked that the atoms are in free fall with no interaction with light for most of the experimental sequence. The very same components are also critical for the thermal aspects. Temperature cooling strategies for the full system[102] or its components need to be considered according to the mass and size budget.

Atom interferometry has the potential to be a cornerstone for a multitude of future space missions as shown in Sec. I B, and in recent years, several European and international projects developed the technology further and performed first demonstrations in relevant environments. However, further development is needed to achieve a sufficient maturity to demonstrate a satellite-borne AI.

Such a process needs to be undertaken at several levels starting with an identification of the mission objectives and of the instrument concept, going through trade-offs at system and mission levels, deriving key technological needs both on the CAI and on the satellite platform. Focused technology development targeting maturation, ruggedization and miniaturization, and the creation of an engineering model that in form, fit, and function is representative of a later flight model. The completion of this process would be a European atom interferometer in-orbit demonstration mission. This goes hand in hand with the creation of an industrial ecosystem including the know-how of the space industry and the development of the related supply chain.

A. Mission and instrument concept definition

Based on the mission scenarios presented in Sec. I D 3, a mission scenario for an in-orbit demonstration needs to be developed, that is, on the one hand, sufficiently comprehensive to demonstrate the necessities for different applications of an atom interferometer (see Sec. II C), and on the other hand, feasible in the sense that only attainable and necessary elements are contained. Such a process should also include a definition of performance requirements and lifetime targets for future missions.

On the basis of this trade-off, satellite and instrument concepts need to be developed that not only include the elements of an atom interferometer presented in Sec. III but also the necessary elements of the satellite platforms. A mission containing an atom interferometer might impose stringent requirement on attitude control, micro vibrations, and orbit determination and possibly necessitate drag compensation. Different platforms have already demonstrated to generate the adequate environment for free-flying masses, from the ISS to The Drag-Free Attitude Control System (DFACS) control put in place by the GOCE mission and in the future probably flying on the Next generation gravity mission (NGGM) mission. These carriers support the payload by providing orbit and attitude maintenance, power, commands, telemetry and data handling, structure, and temperature control.

The process to identify mission scenario and satellite and instrument concept should include the European atom inteferometry community as well as industrial participants concerned with relevant components and space systems.

B. Technology development

After the mission scenario and instrument concepts are agreed upon, it is necessary to identify the directions of technological development and execute them. In Sec. III, development plans for all major subsystems of an AI are outlined. The focus of these developments is on the following aspects:

- Increasing the specific subsystem performance, e.g., atom number for the atom source or number of photon recoils transferred for the interrogation;
- Decreasing power dissipation, mass, and volume;
- Increasing reliably, stability, and autonomy;
- Ruggedizing and, as applicable, qualification of the subsystems in respect to the typical environmental conditions of space-flight, i.e., mechanical and thermal loads, operation in vacuum, and electromagnetic and ionizing radiation.

Here, a focus should be put on solutions suitable for space: for example, rubidium works very well and is far developed; however,

Table IV. List of development plans.

Components	TRL target	Performance goal	Status	References
Miniaturized vacuum chamber including magnetic shield	8	Reduce its contribution to the SWaP budget	In progress: grating MOT, components via additive manufacturing, passive pumping,…	132
Laser system	8	Complete, frequency-agile laser system for cooling and Raman interferometry, including frequency comb / similar reference for gravity gradient compensation	Fibered and fiber (CNES, iXblue)/free-space systems under construction. Fibered system planned for 2025, free-space systems planned for 2022 (MAIUS) and 2026 (BECCAL).	28, 100, 121
All optical atom source (BEC)	5	10^6 Atoms in 1 s	A few 10^4 atoms in 1 s	98
Atom chip source (BEC)	5	$\geq 10^6$ Atoms in 1 s	10^5 Atoms in 1 s	99
Rotation management	5	Control of the reference mirror tilt with a resolution (ideally accuracy) of 10 nrad	Resolution of 1 nrad on ground (static)	184
Gravity gradient management	5	Demonstration in microgravity for a single CAI	Demonstrated on ground for a differential measurement	196
Noninertial acceleration compensation	5	Demonstration at high sensitivity in microgravity	Demonstrated in microgravity at low sensitivity	26
Raman double diffraction in microgravity	5	Increase the efficiency of the atomic beam splitter/mirror using ultra cold atoms	Demonstrated on a gyroscope and a gravimeter with thermal atoms on ground	75
Increase the sensitivity of a single atom interferometer (e.g., optimization of detection, final atom preparation, Raman transitions efficiency)	5	10^{-10} m · s^{-1}· $Hz^{-1/2}$	The best performance on ground is only for a differential measurement	43
Double species atom source	5	Control of the relative position and velocity of two ultracold atom source	Several experiments on ground	219
Multidimensional atom interferometry	5	Measure the three components of the vector accelerometer simultaneously	Only theoretical	72
Detection of the (multiple) output ports		Signal to noise ration better than 1000 with less than 1% crosstalk	State labeling fluorescence demonstrated so far for the double diffraction, spatially resolved detection demonstrated in other architectures	
Atom chips with grating structures	4–5+	BEC with 10^5 atoms/s in a simplified sensor head	In development (TRL 3–4)	
BEC atom interferometer at long free fall times	5+	Free fall time of more than 10 s	2T = 675 ms in drop tower, 2T = 2.3 s in Stanford fountain (TRL 3-4)	15, 17
Double Bragg diffraction	5+	Contrast of 100%	Contrast of 80% on ground (TRL 3)	175
Lasers (780 nm)	5+	800 mW Output at laserhead, 100 kHz linewidth	Tests, qualification for life time, radiation hardness required (TRL 4-5)	9, 108
Electronics	5+	Laser drivers, locks, coil /chip current drivers, AOM drivers,…	Tests, qualification for life time, radiation hardness required (TRL 4-5)	9, 108
Magnetic BEC displacement	5+	Fast, excitation-less transport over a distance of 5 mm and more	Current distance: 1 mm	81
BEC displacement in optical lattice	5+	Bloch-oscillation-based BEC shuttling and launch	Launch in 10 m experiment in Stanford, measurements of fine structure constant	17, 220, 221
Autonomous optimization	5+	Control system for autonomous optimization of experiment	Partial optimization demonstrated on ground (TRL 3-4)	99, 211
Automated image analysis	5+	Automated fit of images to minimize data rate for downlink	Images evaluated after downlink	9, 108

strontium has a smaller sensitivity to magnetic fields, thus, reducing the need of magnetic shielding as a primary mass driver. These developments need to be conducted in close collaboration between academia and industry, with the goal of establishing an industrial or comparable supply chain for the components of an atom interferometer in space.

Complementary to technology developments on the atom interferometer, needs for improvement on the space craft have to be identified and addressed. These include:

- Optimization of spacecraft envelope and shape;
- Consolidation of electric propulsion;
- Optimization of thruster layout;
- Angular rate measurement or reconstruction.

C. Creation of an engineering qualification model

The subsystems further matured in the previous steps should then be joined in an Engineering Qualification Model (EQM). Such a system should be fully representative to a flight model. While not necessarily all components of such an EQM would be flight worthy, they would ideally be in a development stage where achieving flight worthiness does not necessitate changes in the components design. In order to demonstrate the performance of the complete instrument, tests in terrestrial microgravity facilities as described in Sec. III K should be done as well as environmental and lifetime test. During these steps, the hand-over of system responsibility to industry could be undertaken.

With the completion of an EQM, the atom interferometer would be sufficiently mature to start the development of an in-orbit demonstration mission leading into the in-orbit utilization of atom interferometry.

V. CONCLUDING REMARKS

Sven Abend, Baptiste Allard, Aidan S. Arnold, Ticijana Ban, Liam Barry, Baptiste Battelier, Ahmad Bawamia, Quentin Beaufils, Simon Bernon, Andrea Bertoldi, Alexis Bonnin, Philippe Bouyer, Alexandre Bresson, Oliver S. Burrow, Benjamin Canuel, Bruno Desruelle, Giannis Drougakis, René Forsberg, Naceur Gaaloul, Alexandre Gauguet, Matthias Gersemann, Paul F. Griffin, Hendrik Heine, Victoria A. Henderson, Waldemar Herr, Simon Kanthak, Markus Krutzik, Maike D. Lachmann, Roland Lammegger, Werner Magnes, Gaetano Mileti, Morgan W. Mitchell, Sergio Mottini, Dimitris Papazoglou, Franck Pereira dos Santos, Achim Peters, Ernst Rasel, Erling Riis, Christian Schubert, Stephan Tobias Seidel, Guglielmo M. Tino, Mathias Van Den Bossche, Wolf von Klitzing, Andreas Wicht, Marcin Witkowski, Nassim Zahzam, and Michał Zawada

Quantum sensors with cold atoms are currently among the most mature quantum technologies, with a wide variety of applications, ranging from earth observation, gravity mapping, underground survey to advanced navigation. Recent developments, both from academia and industry, have led a to high maturity of compact and/or commercial devices that can operate in a variety of environments, from underground quiet laboratories to moving platform such as boats or planes. Space, where this technology can reach its ultimate performance in terms of sensitivity, is still an open challenge. Many developments, at component or subsystem levels, have recently been achieved thanks to the efforts and supports of space agencies worldwide. With today's availability of many testing platforms that allow the manipulation of ultracold atoms in microgravity and in space, the last phase of early demonstration is just one small step away before future space missions can leap into the Quantum Era.

ACKNOWLEDGMENTS

This roadmap was elaborated in the frame of the European Space Agency (ESA) Contract No. 4000131926/20/NL/AR/idb "Technical Assessment for the Development and Refinement of Techniques and Technologies for Laser Cooled Atomic Inertial Sensors for Space," with the contribution of the COST Action CA16221 "Atom Quantum Technologies" AtomQT and the CNES/DLR collaboration QUANTA.

Members of LP2N, LCAR, LNE-SYRTE, and iXBlue acknowledge support from CNES support for ICE and through R&T program. LP2N and iXBlue are affiliated to the Naquidis[222] Center for Quantum technologies. Members of LP2N acknowledge financial support from the "Agence Nationale pour la Recherche" (grant EOSBECMR No. ANR-18-CE91-0003-01 and grant MIGA No. ANR-11-EQPX-0028).

P.B. acknowledges support by the Dutch National Growth Fund (NGF), as part of the Quantum Delta NL programme.

Members of Leibniz Universität Hannover, Institut für Quantenoptik acknowledge financial support from the German Space Agency (DLR) with funds provided by the Federal Ministry for Economic Affairs and Climate Action (BMWK) due to an enactment of the German Bundestag under Grant No. DLR 50WM1952 "QUANTUS-V Fallturm," 50WM2250A "QUANTUS+," 50WP1431 "QUANTUS-IV MAIUS," 50WM1947 "KACTUS II," 50RK1957 "QGyro," 50NA2106 "QGyro+," 50WM2060 "CARIOQA," 50WM1861 "CAL," 50WM2253A "AI-quadrat" and from "Niedersächsisches Vorab" through the "Quantum- and Nano-Metrology (QUANOMET)" initiative within the project QT3. Additionally, they acknowledge support by the Deutsche Forschungsgemeinschaft (DFG, German Research Foundation)—project-ID 434617780–SFB 1464 TerraQ within the projects A01, A02, A03,—Project-ID 274200144—SFB 1227 DQ-mat within the Projects A05, B07, B09, and under Germany's Excellence Strategy—project-ID 390837967—EXC-2123 Quantum Frontiers.

M.W.M. acknowledges support from NextGenerationEU (PRTR-C17.I1), Generalitat de Catalunya Severo Ochoa: Center of Excellence CEX2019-000910-S, CERCA program, AGAUR Grant No. 2017-SGR-1354, project SAPONARIA (PID2021-123813NB-I00) funded by MCIN/AEI/10.13039/501100011033/FEDER, Fundació Privada Cellex; Fundació Mir-Puig.

AUTHOR DECLARATIONS

Conflict of Interest

The authors have no conflicts to disclose.

Author Contributions

Sven Abend: Writing – original draft (equal); Writing – review & editing (equal). **Andrea Bertoldi:** Writing – original draft (equal); Writing – review & editing (equal). **Alexis Bonnin:** Writing – original draft (equal); Writing – review & editing (equal). **Philippe Bouyer:** Writing – original draft (lead); Writing – review & editing (lead). **Alexandre Bresson:** Writing – original draft (equal); Writing – review & editing (equal). **Oliver Burrow:** Writing – original draft (equal); Writing – review & editing (equal). **Benjamin Canuel:** Writing – original draft (equal); Writing – review & editing (equal). **Bruno Desruelle:** Writing – original draft (equal); Writing – review & editing (equal). **Giannis Drougakis:** Writing – original draft (equal); Writing – review & editing (equal). **Rene Forsberg:** Writing – original draft (equal); Writing – review & editing (equal). **Naceur Gaaloul:** Writing – original draft (equal); Writing – review & editing (equal). **Baptiste Allard:** Writing – original draft (equal); Writing – review & editing (equal). **Alexandre Gauguet:** Writing – original draft (equal); Writing – review & editing (equal). **Matthias Gersemann:** Writing – original draft (equal); Writing – review & editing (equal). **Paul F. Griffin:** Writing – original draft (equal); Writing – review & editing (equal). **Hendrik Heine:** Writing – original draft (equal); Writing – review & editing (equal). **Victoria A. Henderson:** Writing – original draft (equal); Writing – review & editing (equal). **Waldemar Herr:** Writing – original draft (equal); Writing – review & editing (equal). **Simon Kanthak:** Writing – original draft (equal); Writing – review & editing (equal). **Markus Krutzik:** Writing – original draft (equal); Writing – review & editing (equal). **Maike Diana Lachmann:** Writing – original draft (equal); Writing – review & editing (equal). **Roland Lammegger:** Writing – original draft (equal); Writing – review & editing (equal). **Aidan S. Arnold:** Writing – original draft (equal); Writing – review & editing (equal). **Magnes:** Writing – original draft (equal); Writing – review & editing (equal). **Gaetano Mileti:** Writing – original draft (equal); Writing – review & editing (equal). **Morgan Wilfred Mitchell:** Writing – original draft (equal); Writing – review & editing (equal). **Sergio Mottini:** Writing – original draft (equal); Writing – review & editing (equal). **Dimitris Papazoglou:** Writing – original draft (equal); Writing – review & editing (equal). **Franck Pereira Dos Santos:** Writing – original draft (equal); Writing – review & editing (equal). **Achim Peters:** Writing – original draft (equal); Writing – review & editing (equal). **Ernst Rasel:** Writing – original draft (equal); Writing – review & editing (equal). **Erling Riis:** Writing – original draft (equal); Writing – review & editing (equal). **Christian Schubert:** Writing – original draft (equal); Writing – review & editing (equal). **Ticijana Ban:** Writing – original draft (equal); Writing – review & editing (equal). **Stephan Seidel:** Writing – original draft (equal); Writing – review & editing (equal). **Guglielmo Maria Tino:** Writing – original draft (equal); Writing – review & editing (equal). **Mathias van den Bossche:** Writing – original draft (equal); Writing – review & editing (equal). **Wolf von Klitzing:** Writing – original draft (equal); Writing – review & editing (equal). **Andreas Wicht:** Writing – original draft (equal); Writing – review & editing (equal). **Marcin Witkowski:** Writing – original draft (equal); Writing – review & editing (equal). **Nassim Zahzam:** Writing – original draft (equal); Writing – review & editing (equal). **Michal Zawada:** Writing – original draft (equal); Writing – review & editing (equal). **Liam Barry:** Writing – original draft (equal); Writing – review & editing (equal). **Baptiste Battelier:** Writing – original draft (equal); Writing – review & editing (equal). **Ahmad Bawamia:** Writing – original draft (equal); Writing – review & editing (equal). **Quentin Beaufils:** Writing – original draft (equal); Writing – review & editing (equal). **Simon Bernon:** Writing – original draft (equal); Writing – review & editing (equal).

DATA AVAILABILITY

Data sharing is not applicable to this article as no new data were created or analyzed in this study.

REFERENCES

[1]S. Chu, Rev. Mod. Phys. **70**, 685 (1998).
[2]C. N. Cohen-Tannoudji, Rev. Mod. Phys. **70**, 707 (1998).
[3]W. D. Phillips, Rev. Mod. Phys. **70**, 721 (1998).
[4]E. A. Cornell and C. E. Wieman, Rev. Mod. Phys. **74**, 875 (2002).
[5]W. Ketterle, Rev. Mod. Phys. **74**, 1131 (2002).
[6]T. Lévèque, B. Faure, F. X. Esnault, C. Delaroche, D. Massonnet, O. Grosjean, F. Buffe, P. Torresi, T. Bomer, A. Pichon, P. Béraud, J. P. Lelay, S. Thomin, and P. Laurent, Rev. Sci. Instrum. **86**, 033104 (2015).
[7]C. Jentsch, T. Müller, E. M. Rasel, and W. Ertmer, Gen. Relativ. Gravitation **36**, 2197 (2004).
[8]R. Geiger, V. Ménoret, G. Stern, N. Zahzam, P. Cheinet, B. Battelier, A. Villing, F. Moron, M. Lours, Y. Bidel, A. Bresson, A. Landragin, and P. Bouyer, Nat. Commun. **2**, 474 (2011).
[9]D. Becker, M. D. Lachmann, S. T. Seidel, H. Ahlers, A. N. Dinkelaker, J. Grosse, O. Hellmig, H. Müntinga, V. Schkolnik, T. Wendrich, A. Wenzlawski, B. Weps, R. Corgier, T. Franz, N. Gaaloul, W. Herr, D. Lüdtke, M. Popp, S. Amri, H. Duncker, M. Erbe, A. Kohfeldt, A. Kubelka-Lange, C. Braxmaier, E. Charron, W. Ertmer, M. Krutzik, C. Lämmerzahl, A. Peters, W. P. Schleich, K. Sengstock, R. Walser, A. Wicht, P. Windpassinger, and E. M. Rasel, Nature **562**, 391 (2018).
[10]D. C. Aveline, J. R. Williams, E. R. Elliott, C. Dutenhoffer, J. R. Kellogg, J. M. Kohel, N. E. Lay, K. Oudrhiri, R. F. Shotwell, N. Yu, and R. J. Thompson, Nature **582**, 193 (2020).
[11]X. Chen and B. Fan, Rep. Prog. Phys. **83**, 076401 (2020).
[12]Y. L. Coq, J. Retter, S. Richard, A. Aspect, and P. Bouyer, Appl. Phys. B **84**, 627 (2006).
[13]B. Barrett, P.-A. Gominet, E. Cantin, L. Antoni-Micollier, A. Bertoldi, B. Battelier, P. Bouyer, J. Lautier, and A. Landragin, *Proceedings of the International School of Physics "Enrico Fermi,"* edited by G. M. Tino and M. A. Kasevich (IOS, Amsterdam, 2014), Vol. 188.
[14]K. Bongs, M. Holynski, J. Vovrosh, P. Bouyer, G. Condon, E. Rasel, C. Schubert, W. P. Schleich, and A. Roura, Nat. Rev. Phys. **1**, 731 (2019).
[15]H. Müntinga, H. Ahlers, M. Krutzik, A. Wenzlawski, S. Arnold, D. Becker, K. Bongs, H. Dittus, H. Duncker, N. Gaaloul, C. Gherasim, E. Giese, C. Grzeschik, T. W. Hänsch, O. Hellmig, W. Herr, S. Herrmann, E. Kajari, S. Kleinert, C. Lämmerzahl, W. Lewoczko-Adamczyk, J. Malcolm, N. Meyer, R. Nolte, A. Peters, M. Popp, J. Reichel, A. Roura, J. Rudolph, M. Schiemangk, M. Schneider, S. T. Seidel, K. Sengstock, V. Tamma, T. Valenzuela, A. Vogel, R. Walser, T. Wendrich, P. Windpassinger, W. Zeller, T. van Zoest, W. Ertmer, W. P. Schleich, and E. M. Rasel, Phys. Rev. Lett. **110**, 093602 (2013).
[16]G. M. Tino, F. Sorrentino, D. Aguilera, B. Battelier, A. Bertoldi, Q. Bodart, K. Bongs, P. Bouyer, C. Braxmaier, L. Cacciapuoti, N. Gaaloul, N. Gürlebeck, M. Hauth, S. Herrmann, M. Krutzik, A. Kubelka, A. Landragin, A. Milke, A. Peters, E. M. Rasel, C. Rocco, E. Schubert, T. Schuldt, K. Sengstock, and A. Wicht, Nucl. Phys. B **243–244**, 203 (2013).
[17]S. M. Dickerson, J. M. Hogan, A. Sugarbaker, D. M. S. Johnson, and M. A. Kasevich, Phys. Rev. Lett. **111**, 083001 (2013).
[18]T. Lévèque, C. Fallet, M. Mandea, R. Biancale, J. M. Lemoine, S. Tardivel, S. Delavault, A. Piquereau, S. Bourgogne, F. P. D. Santos, B. Battelier, and P. Bouyer, J. Geod. **95**, 15 (2021).
[19]Encyclopedia of Geodesy, *Encyclopedia of Earth Sciences Series*, edited by M. G. Sideris (Springer International Publishing Cham, New York, 2020).

[20]P. Touboul, B. Foulon, M. Rodrigues, and J. P. Marque, Aerosp. Sci. Technol. **8**, 431 (2004).
[21]G. Beutler, M. Drinkwater, R. Rummel, and R. von Steiger, *Earth Gravity Field From Space-From Sensors to Earth Sciences*, Space Sciences Series of ISSI (Springer, Netherlands, 2003).
[22]Y. Bidel, N. Zahzam, A. Bresson, C. Blanchard, M. Cadoret, A. V. Olesen, and R. Forsberg, J. Geod. **94**, 20 (2020).
[23]See https://www.qureca.com/overview-on-quantum-initiatives-worldwide-update-mid-2021/ for "Qureca Overview on Quantum Initiatives" (2021), and references therein.
[24]F. Sorrentino, K. Bongs, P. Bouyer, L. Cacciapuoti, M. d Angelis, H. Dittus, W. Ertmer, J. Hartwig, M. Hauth, S. Herrmann, K. Huang, M. Inguscio, E. Kajari, T. Könemann, C. Lämmerzahl, A. Landragin, G. Modugno, F. P. d. Santos, A. Peters, M. Prevedelli, E. M. Rasel, W. P. Schleich, M. Schmidt, A. Senger, K. Sengstock, G. Stern, G. M. Tino, T. Valenzuela, R. Walser, and P. Windpassinger, J. Phys. **327**, 012050 (2011).
[25]D. N. Aguilera, H. Ahlers, B. Battelier, A. Bawamia, A. Bertoldi, R. Bondarescu, K. Bongs, P. Bouyer, C. Braxmaier, L. Cacciapuoti, C. Chaloner, M. Chwalla, W. Ertmer, M. Franz, N. Gaaloul, M. Gehler, D. Gerardi, L. Gesa, N. Gürlebeck, J. Hartwig, M. Hauth, O. Hellmig, W. Herr, S. Herrmann, A. Heske, A. Hinton, P. Ireland, P. Jetzer, U. Johann, M. Krutzik, A. Kubelka, C. Lämmerzahl, A. Landragin, I. Lloro, D. Massonnet, I. Mateos, A. Milke, M. Nofrarias, M. Oswald, A. Peters, K. Posso-Trujillo, E. Rasel, E. Rocco, A. Roura, J. Rudolph, W. Schleich, C. Schubert, T. Schuldt, S. Seidel, K. Sengstock, C. F. Sopuerta, F. Sorrentino, D. Summers, G. M. Tino, C. Trenkel, N. Uzunoglu, W. von Klitzing, R. Walser, T. Wendrich, A. Wenzlawski, P. Weßels, A. Wicht, E. Wille, M. Williams, P. Windpassinger, and N. Zahzam, Classical Quantum Gravity **31**, 115010 (2014).
[26]B. Barrett, L. Antoni-Micollier, L. Chichet, B. Battelier, T. Lévèque, A. Landragin, and P. Bouyer, Nat. Commun. **7**, 13786 (2016).
[27]E. R. Elliott, M. C. Krutzik, J. R. Williams, R. J. Thompson, and D. C. Aveline, npj Microgravity **4**, 16 (2018).
[28]K. Frye, S. Abend, W. Bartosch, A. Bawamia, D. Becker, H. Blume, C. Braxmaier, S.-W. Chiow, M. A. Efremov, W. Ertmer, P. Fierlinger, T. Franz, N. Gaaloul, J. Grosse, C. Grzeschik, O. Hellmig, V. A. Henderson, W. Herr, U. Israelsson, J. Kohel, M. Krutzik, C. Kürbis, C. Lämmerzahl, M. List, D. Lüdtke, N. Lundblad, J. P. Marburger, M. Meister, M. Mihm, H. Müller, H. Müntinga, A. M. Nepal, T. Oberschulte, A. Papakonstantinou, J. Perovsek, A. Peters, A. Prat, E. M. Rasel, A. Roura, M. Sbroscia, W. P. Schleich, C. Schubert, S. T. Seidel, J. Sommer, C. Spindeldreier, D. Stamper-Kurn, B. K. Stuhl, M. Warner, T. Wendrich, A. Wenzlawski, A. Wicht, P. Windpassinger, N. Yu, and L. Wörner, EPJ Quantum Technol. **8**, 1 (2021).
[29]B. Battelier, J. Bergé, A. Bertoldi, L. Blanchet, K. Bongs, P. Bouyer, C. Braxmaier, D. Calonico, P. Fayet, N. Gaaloul, C. Guerlin, A. Hees, P. Jetzer, C. Lämmerzahl, S. Lecomte, C. L. Poncin-Lafitte, S. Loriani, G. Métris, M. Nofrarias, E. Rasel, S. Reynaud, M. Rodrigues, M. Rothacher, A. Roura, C. Salomon, S. Schiller, W. P. Schleich, C. Schubert, C. F. Sopuerta, F. Sorrentino, T. J. Sumner, G. M. Tino, P. Tuckey, W. von Klitzing, L. Wörner, P. Wolf, and M. Zelan, Exp. Astron. **51**, 1695 (2021).
[30]Y. A. El-Neaj, C. Alpigiani, S. Amairi-Pyka, H. Araújo, A. Balaž, A. Bassi, L. Bathe-Peters, B. Battelier, A. Belić, E. Bentine, J. Bernabeu, A. Bertoldi, R. Bingham, D. Blas, V. Bolpasi, K. Bongs, S. Bose, P. Bouyer, T. Bowcock, W. Bowden, O. Buchmueller, C. Burrage, X. Calmet, B. Canuel, L.-I. Caramete, A. Carroll, G. Cella, V. Charmandaris, S. Chattopadhyay, X. Chen, M. L. Chiofalo, J. Coleman, J. Cotter, Y. Cui, A. Derevianko, A. D. Roeck, G. S. Djordjevic, P. Dornan, M. Doser, I. Drougkakis, J. Dunningham, I. Dutan, S. Easo, G. Elertas, J. Ellis, M. E. Sawy, F. Fassi, D. Felea, C.-H. Feng, R. Flack, C. Foot, I. Fuentes, N. Gaaloul, A. Gauguet, R. Geiger, V. Gibson, G. Giudice, J. Goldwin, O. Grachov, P. W. Graham, D. Grasso, M. van der Grinten, M. Gündogan, M. G. Haehnelt, T. Harte, A. Hees, R. Hobson, J. Hogan, B. Holst, M. Holynski, M. Kasevich, B. J. Kavanagh, W. von Klitzing, T. Kovachy, B. Krikler, M. Krutzik, M. Lewicki, Y.-H. Lien, M. Liu, G. G. Luciano, A. Magnon, M. A. Mahmoud, S. Malik, C. McCabe, J. Mitchell, J. Pahl, D. Pal, S. Pandey, D. Papazoglou, M. Paternostro, B. Penning, A. Peters, M. Prevedelli, V. Puthiya-Veettil, J. Quenby, E. Rasel, S. Ravenhall, J. Ringwood, A. Roura, D. Sabulsky, M. Sameed, B. Sauer, S. A. Schäffer, S. Schiller, V. Schkolnik, D. Schlippert, C. Schubert, H. R. Sfar, A. Shayeghi, I. Shipsey, C. Signorini, Y. Singh, M. Soares-Santos, F. Sorrentino, T. Sumner, K. Tassis, S. Tentindo, G. M. Tino, J. N. Tinsley, J. Unwin, T. Valenzuela, G. Vasilakis, V. Vaskonen, C. Vogt, A. Webber-Date, A. Wenzlawski, P. Windpassinger, M. Woltmann, E. Yazgan, M.-S. Zhan, X. Zou, and J. Zupan, EPJ Quantum Technol. **7**, 6 (2020).
[31]G. M. Tino, A. Bassi, G. Bianco, K. Bongs, P. Bouyer, L. Cacciapuoti, S. Capozziello, X. Chen, M. L. Chiofalo, A. Derevianko, W. Ertmer, N. Gaaloul, P. Gill, P. W. Graham, J. M. Hogan, L. Iess, M. A. Kasevich, H. Katori, C. Klempt, X. Lu, L.-S. Ma, H. Müller, N. R. Newbury, C. W. Oates, A. Peters, N. Poli, E. M. Rasel, G. Rosi, A. Roura, C. Salomon, S. Schiller, W. Schleich, D. Schlippert, F. Schreck, C. Schubert, F. Sorrentino, U. Sterr, J. W. Thomsen, G. Vallone, F. Vetrano, P. Villoresi, W. von Klitzing, D. Wilkowski, P. Wolf, J. Ye, N. Yu, and M. Zhan, Eur. Phys. J. D **73**, 228 (2019).
[32]G. Wang, D. Gao, W.-T. Ni, J. Wang, and M. Zhan, Int. Mod. Phys. D **29**, 1940004 (2020).
[33]O. Carraz, C. Siemes, L. Massotti, R. Haagmans, and P. Silvestrin, Microgravity Sci. Technol. **26**, 139 (2014).
[34]K. Douch, H. Wu, C. Schubert, J. Müller, and F. Pereira dos Santos, Adv. Space Res. **61**, 1307 (2018).
[35]A. Trimeche, B. Battelier, D. Becker, A. Bertoldi, P. Bouyer, C. Braxmaier, E. Charron, R. Corgier, M. Cornelius, K. Douch, N. Gaaloul, S. Herrmann, J. Müller, E. Rasel, C. Schubert, H. Wu, and F. Pereira dos Santos, Classical Quantum. Gravity **36**, 215004 (2019).
[36]X. Chen, H. Li, J. Yu, B. Fan, W. Xiong, Y. Zhang, X. Yuan, S. Yang, Q. Huang, R. Liao, J. Zhao, L. Liang, Q. Zheng, X. Zhou, B. Wang, D. Chen, L. Liu, W. Chen, M. Liu, and Z. Ma, Cold-Atom On-Line Meeting 2020 (2020).
[37]P. Abrykosov, R. Pail, T. Gruber, N. Zahzam, A. Bresson, E. Hardy, B. Christophe, Y. Bidel, O. Carraz, and C. Siemes, Adv. Space Res. **63**, 3235 (2019).
[38]C. M. Will, Living Rev. Relativ. **9**, 3 (2006).
[39]T. Damour, F. Piazza, and G. Veneziano, Phys. Rev. D **66**, 046007 (2002).
[40]S. Schlamminger, K.-Y. Choi, T. A. Wagner, J. H. Gundlach, and E. G. Adelberger, Phys. Rev. Lett. **100**, 041101 (2008).
[41]J. G. Williams, S. G. Turyshev, and D. H. Boggs, Phys. Rev. Lett. **93**, 261101 (2004).
[42]P. Touboul, G. Métris, M. Rodrigues, Y. André, Q. Baghi, J. Bergé, D. Boulanger, S. Bremer, P. Carle, R. Chhun, B. Christophe, V. Cipolla, T. Damour, P. Danto, H. Dittus, P. Fayet, B. Foulon, C. Gageant, P.-Y. Guidotti, D. Hagedorn, E. Hardy, P.-A. Huynh, H. Inchauspe, P. Kayser, S. Lala, C. Lämmerzahl, V. Lebat, P. Leseur, F. Liorzou, M. List, F. Löffler, I. Panet, B. Pouilloux, P. Prieur, A. Rebray, S. Reynaud, B. Rievers, A. Robert, H. Selig, L. Serron, T. Sumner, N. Tanguy, and P. Visser, Phys. Rev. Lett. **119**, 231101 (2017).
[43]P. Asenbaum, C. Overstreet, M. Kim, J. Curti, and M. A. Kasevich, Phys. Rev. Lett. **125**, 191101 (2020).
[44]L. Zhou, S. Long, B. Tang, X. Chen, F. Gao, W. Peng, W. Duan, J. Zhong, Z. Xiong, J. Wang, Y. Zhang, and M. Zhan, Phys. Rev. Lett. **115**, 013004 (2015).
[45]L. Zhou, C. He, S.-T. Yan, X. Chen, D.-F. Gao, W.-T. Duan, Y.-H. Ji, R.-D. Xu, B. Tang, C. Zhou, S. Barthwal, Q. Wang, Z. Hou, Z.-Y. Xiong, Y.-Z. Zhang, M. Liu, W.-T. Ni, J. Wang, and M.-S. Zhan, Phys. Rev. A **104**, 022822 (2021).
[46]G. Rosi, G. D'Amico, L. Cacciapuoti, F. Sorrentino, M. Prevedelli, M. Zych, Č. Brukner, and G. M. Tino, Nat. Commun. **8**, 15529 (2017).
[47]B. Barrett, G. Condon, L. Chichet, L. Antoni-Micollier, R. Arguel, M. Rabault, C. Pelluet, V. Jarlaud, A. Landragin, P. Bouyer, and B. Battelier, AVS Quantum Sci. **4**, 014401 (2022).
[48]D. Schlippert, J. Hartwig, H. Albers, L. L. Richardson, C. Schubert, A. Roura, W. P. Schleich, W. Ertmer, and E. M. Rasel, Phys. Rev. Lett. **112**, 203002 (2014).
[49]T. Kovachy, J. M. Hogan, A. Sugarbaker, S. M. Dickerson, C. A. Donnelly, C. Overstreet, and M. A. Kasevich, Phys. Rev. Lett. **114**, 143004 (2015).
[50]J. Grosse, S. T. Seidel, D. Becker, M. D. Lachmann, M. Scharringhausen, C. Braxmaier, and E. M. Rasel, J. Vac. Sci. Technol. A **34**, 031606 (2016).
[51]A. N. Dinkelaker, M. Schiemangk, V. Schkolnik, A. Kenyon, K. Lampmann, A. Wenzlawski, P. Windpassinger, O. Hellmig, T. Wendrich, E. M. Rasel, M. Giunta, C. Deutsch, C. Kürbis, R. Smol, A. Wicht, M. Krutzik, and A. Peters, Appl. Opt. **56**, 1388 (2017).

[52]F. Migliaccio, M. Reguzzoni, K. Batsukh, G. M. Tino, G. Rosi, F. Sorrentino, C. Braitenberg, T. Pivetta, D. F. Barbolla, and S. Zoffoli, Surv. Geophys. **40**, 1029 (2019).
[53]T. Lévèque, C. Fallet, M. Mandea, R. Biancale, J. M. Lemoine, S. Tardivel, M. Delpech, G. Ramillien, J. Panet, S. Bourgogne, F. Pereira Dos Santos, and P. Bouyer, Proc. SPIE **11180**, 111800W (2019).
[54]J. Le Gouët, T. Mehlstäubler, J. Kim, S. Merlet, A. Clairon, A. Landragin, and F. Pereira Dos Santos, Appl. Phys. B **92**, 133 (2008).
[55]Y. Bidel, N. Zahzam, C. Blanchard, A. Bonnin, M. Cadoret, A. Bresson, D. Rouxel, and M. F. Lequentrec-Lalancette, Nat. Commun. **9**, 627 (2018).
[56]See https://science.nasa.gov/earth-science/decadal-surveys/ for "NASA Decadal Survey" (2021).
[57]See https://www.horizon-europe.gouv.fr/quantum-technologies-space-gravimetry-25964 for "EU Call for Space Atom Gradiometer" (2021).
[58]S.-W. Chiow, T. Kovachy, H.-C. Chien, and M. A. Kasevich, Phys. Rev. Lett. **107**, 130403 (2011).
[59]M. Kasevich and S. Chu, Appl. Phys. B **54**, 321 (1992).
[60]F. Riehle, T. Kisters, A. Witte, J. Helmcke, and C. J. Bordé, Phys. Rev. Lett. **67**, 177 (1991).
[61]S. Merlet, A. Kopaev, M. Diament, G. Geneves, A. Landragin, and F. P. D. Santos, Metrologia **45**, 265 (2008).
[62]M. J. Snadden, J. M. McGuirk, P. Bouyer, K. G. Haritos, and M. A. Kasevich, Phys. Rev. Lett. **81**, 971 (1998).
[63]A. Bertoldi, G. Lamporesi, L. Cacciapuoti, M. de Angelis, M. Fattori, T. Petelski, A. Peters, M. Prevedelli, J. Stuhler, and G. M. Tino, Eur. Phys. J. D **40**, 271 (2006).
[64]J. B. Fixler, G. T. Foster, J. M. McGuirk, and M. A. Kasevich, Science **315**, 74 (2007).
[65]G. Lamporesi, A. Bertoldi, L. Cacciapuoti, M. Prevedelli, and G. M. Tino, Phys. Rev. Lett. **100**, 050801 (2008).
[66]G. Rosi, F. Sorrentino, L. Cacciapuoti, M. Prevedelli, and G. M. Tino, Nature **510**, 518 (2014).
[67]S. Dimopoulos, P. W. Graham, J. M. Hogan, M. A. Kasevich, and S. Rajendran, Phys. Rev. D **78**, 122002 (2008).
[68]B. Canuel, A. Bertoldi, L. Amand, E. P. di Borgo, T. Chantrait, C. Danquigny, M. D. Álvarez, B. Fang, A. Freise, R. Geiger, J. Gillot, S. Henry, J. Hinderer, D. Holleville, J. Junca, G. Lefèvre, M. Merzougui, N. Mielec, T. Monfret, S. Pelisson, M. Prevedelli, S. Reynaud, I. Riou, Y. Rogister, S. Rosat, E. Cormier, A. Landragin, W. Chaibi, S. Gaffet, and P. Bouyer, Sci. Rep. **8**, 14064 (2018).
[69]W. Chaibi, R. Geiger, B. Canuel, A. Bertoldi, A. Landragin, and P. Bouyer, Phys. Rev. D **93**, 021101 (2016).
[70]J. M. Hogan, D. M. S. Johnson, S. Dickerson, T. Kovachy, A. Sugarbaker, S.-W. Chiow, P. W. Graham, M. A. Kasevich, B. Saif, S. Rajendran, P. Bouyer, B. D. Seery, L. Feinberg, and R. Keski-Kuha, Gen. Relativ. Gravit. B, 1953–2009 (2011).
[71]D. Savoie, M. Altorio, B. Fang, L. A. Sidorenkov, R. Geiger, and A. Landragin, Sci. Adv. **4**, eaau7948 (2018).
[72]B. Barrett, P. Cheiney, B. Battelier, F. Napolitano, and P. Bouyer, Phys. Rev. Lett. **122**, 043604 (2019).
[73]M. Gersemann, M. Gebbe, S. Abend, C. Schubert, and E. M. Rasel, Eur. Phys. J. D **74**, 203 (2020).
[74]P. Berg, S. Abend, G. Tackmann, C. Schubert, E. Giese, W. Schleich, F. Narducci, W. Ertmer, and E. Rasel, Phys. Rev. Lett. **114**, 063002 (2015).
[75]T. Lévèque, A. Gauguet, F. Michaud, F. Pereira Dos Santos, and A. Landragin, Phys. Rev. Lett. **103**, 080405 (2009).
[76]E. Giese, A. Roura, G. Tackmann, E. M. Rasel, and W. P. Schleich, Phys. Rev. A **88**, 053608 (2013).
[77]H. Ahlers, H. Müntinga, A. Wenzlawski, M. Krutzik, G. Tackmann, S. Abend, N. Gaaloul, E. Giese, A. Roura, R. Kuhl, C. Lämmerzahl, A. Peters, P. Windpassinger, K. Sengstock, W. Schleich, W. Ertmer, and E. Rasel, Phys. Rev. Lett. **116**, 173601 (2016).
[78]H. Ammann and N. Christensen, Phys. Rev. Lett. **78**, 2088 (1997).
[79]A. S. Arnold, C. MacCormick, and M. G. Boshier, Phys. Rev. A **65**, 031601 (2002).
[80]A. S. Arnold, C. MacCormick, and M. G. Boshier, J. Phys. B **37**, 485 (2004).
[81]C. Deppner, W. Herr, M. Cornelius, P. Stromberger, T. Sternke, C. Grzeschik, A. Grote, J. Rudolph, S. Herrmann, M. Krutzik, A. Wenzlawski, R. Corgier, E. Charron, D. Guéry-Odelin, N. Gaaloul, C. Lämmerzahl, A. Peters, P. Windpassinger, and E. M. Rasel, Phys. Rev. Lett. **127**, 100401 (2021).
[82]G. Sechi, M. Buonocore, F. Cometto, M. Saponara, A. Tramutola, B. Vinai, G. Andrè, and M. Fehringer, IFAC Proc. **44**, 733 (2011).
[83]T. Kovachy, P. Asenbaum, C. Overstreet, C. A. Donnelly, S. M. Dickerson, A. Sugarbaker, J. M. Hogan, and M. A. Kasevich, Nature **528**, 530 (2015).
[84]M. Armano, H. Audley, G. Auger, J. T. Baird, M. Bassan, P. Binetruy, M. Born, D. Bortoluzzi, N. Brandt, M. Caleno, L. Carbone, A. Cavalleri, A. Cesarini, G. Ciani, G. Congedo, A. M. Cruise, K. Danzmann, M. de Deus Silva, R. De Rosa, M. Diaz-Aguiló, L. Di Fiore, I. Diepholz, G. Dixon, R. Dolesi, N. Dunbar, L. Ferraioli, V. Ferroni, W. Fichter, E. D. Fitzsimons, R. Flatscher, M. Freschi, A. F. García Marín, C. García Marirrodriga, R. Gerndt, L. Gesa, F. Gibert, D. Giardini, R. Giusteri, F. Guzmán, A. Grado, C. Grimani, A. Grynagier, J. Grzymisch, I. Harrison, G. Heinzel, M. Hewitson, D. Hollington, D. Hoyland, M. Hueller, H. Inchauspé, O. Jennrich, P. Jetzer, U. Johann, B. Johlander, N. Karnesis, B. Kaune, N. Korsakova, C. J. Killow, J. A. Lobo, I. Lloro, L. Liu, J. P. López-Zaragoza, R. Maarschalkerweerd, D. Mance, V. Martín, L. Martin-Polo, J. Martino, F. Martin-Porqueras, S. Madden, I. Mateos, P. W. McNamara, J. Mendes, L. Mendes, A. Monsky, D. Nicolodi, M. Nofrarias, S. Paczkowski, M. Perreur-Lloyd, A. Petiteau, P. Pivato, E. Plagnol, P. Prat, U. Ragnit, B. Raïs, J. Ramos-Castro, J. Reiche, D. I. Robertson, H. Rozemeijer, F. Rivas, G. Russano, J. Sanjuán, P. Sarra, A. Schleicher, D. Shaul, J. Slutsky, C. F. Sopuerta, R. Stanga, F. Steier, T. Sumner, D. Texier, J. I. Thorpe, C. Trenkel, M. Tröbs, H. B. Tu, D. Vetrugno, S. Vitale, V. Wand, G. Wanner, H. Ward, C. Warren, P. J. Wass, D. Wealthy, W. J. Weber, L. Wissel, A. Wittchen, A. Zambotti, C. Zanoni, T. Ziegler, and P. Zweifel, Phys. Rev. Lett. **116**, 231101 (2016).
[85]M. Armano, H. Audley, J. Baird, P. Binetruy, M. Born, D. Bortoluzzi, E. Castelli, A. Cavalleri, A. Cesarini, A. Cruise, K. Danzmann, M. de Deus Silva, I. Diepholz, G. Dixon, R. Dolesi, L. Ferraioli, V. Ferroni, E. Fitzsimons, M. Freschi, L. Gesa, F. Gibert, D. Giardini, R. Giusteri, C. Grimani, J. Grzymisch, I. Harrison, G. Heinzel, M. Hewitson, D. Hollington, D. Hoyland, M. Hueller, H. Inchauspé, O. Jennrich, P. Jetzer, N. Karnesis, B. Kaune, N. Korsakova, C. Killow, J. Lobo, I. Lloro, L. Liu, J. López-Zaragoza, R. Maarschalkerweerd, D. Mance, N. Meshksar, V. Martín, L. Martin-Polo, J. Martino, F. Martin-Porqueras, I. Mateos, P. McNamara, J. Mendes, L. Mendes, M. Nofrarias, S. Paczkowski, M. Perreur-Lloyd, A. Petiteau, P. Pivato, E. Plagnol, J. Ramos-Castro, J. Reiche, D. Robertson, F. Rivas, G. Russano, J. Slutsky, C. Sopuerta, T. Sumner, D. Texier, J. Thorpe, D. Vetrugno, S. Vitale, G. Wanner, H. Ward, P. Wass, W. Weber, L. Wissel, A. Wittchen, and P. Zweifel, Phys. Rev. Lett. **120**, 061101 (2018).
[86]E. Savalle, C. Guerlin, P. Delva, F. Meynadier, C. le Poncin-Lafitte, and P. Wolf, Classical Quantum Gravity **36**, 245004 (2019).
[87]K.-Y. Chung, S-w Chiow, S. Herrmann, S. Chu, and H. Müller, Phys. Rev. D **80**, 016002 (2009).
[88]Z. Wang, L. Shao, and C. Liu, Astrophys. J. **921**, 158 (2021).
[89]LISA Consortium, *LISA: Assessment Study Report* (LISA Consortium, 2011).
[90]B. Elder, J. Khoury, P. Haslinger, M. Jaffe, H. Müller, and P. Hamilton, Phys. Rev. D **94**, 044051 (2016).
[91]S.-W. Chiow and N. Yu, Phys. Rev. D **101**, 083501 (2020).
[92]P. Hamilton, M. Jaffe, P. Haslinger, Q. Simmons, H. Müller, and J. Khoury, Science **349**, 849 (2015).
[93]M. Jaffe, P. Haslinger, V. Xu, P. Hamilton, A. Upadhye, B. Elder, J. Khoury, and H. Müller, Nat. Phys. **13**, 938 (2017).
[94]D. O. Sabulsky, I. Dutta, E. A. Hinds, B. Elder, C. Burrage, and E. J. Copeland, Phys. Rev. Lett. **123**, 061102 (2019).
[95]G. C. Ghirardi, A. Rimini, and T. Weber, Phys. Rev. D **34**, 470 (1986).
[96]A. Bassi, K. Lochan, S. Satin, T. P. Singh, and H. Ulbricht, Rev. Mod. Phys. **85**, 471 (2013).
[97]S. Nimmrichter and K. Hornberger, Phys. Rev. Lett. **110**, 160403 (2013).
[98]G. Condon, M. Rabault, B. Barrett, L. Chichet, R. Arguel, H. Eneriz-Imaz, D. Naik, A. Bertoldi, B. Battelier, P. Bouyer, and A. Landragin, Phys. Rev. Lett. **123**, 240402 (2019).
[99]J. Rudolph, W. Herr, C. Grzeschik, T. Sternke, A. Grote, M. Popp, D. Becker, H. Müntinga, H. Ahlers, A. Peters, C. Lämmerzahl, K. Sengstock, N. Gaaloul, W. Ertmer, and E. M. Rasel, New J. Phys. **17**, 065001 (2015).
[100]V. Schkolnik, O. Hellmig, A. Wenzlawski, J. Grosse, A. Kohfeldt, K. Döringshoff, A. Wicht, P. Windpassinger, K. Sengstock, C. Braxmaier, M. Krutzik, and A. Peters, Appl. Phys. B **122**, 217 (2016).

[101]R. Caldani, S. Merlet, F. Pereira Dos Santos, G. Stern, A.-S. Martin, B. Desruelle, and V. Ménoret, Eur. Phys. J. D **73**, 248 (2019).
[102]D. O. Sabulsky, J. Junca, G. Lefèvre, X. Zou, A. Bertoldi, B. Battelier, M. Prevedelli, G. Stern, J. Santoire, Q. Beaufils, R. Geiger, A. Landragin, B. Desruelle, P. Bouyer, and B. Canuel, Sci. Rep. **10**, 3268 (2020).
[103]O. S. Burrow, P. F. Osborn, E. Boughton, F. Mirando, D. P. Burt, P. F. Griffin, A. S. Arnold, and E. Riis, Appl. Phys. Lett. **119**, 124002 (2021).
[104]J. P. McGilligan, K. R. Moore, A. Dellis, G. D. Martinez, E. de Clercq, P. F. Griffin, A. S. Arnold, E. Riis, R. Boudot, and J. Kitching, Appl. Phys. Lett. **117**, 054001 (2020).
[105]B. J. Little, G. W. Hoth, J. Christensen, C. Walker, D. J. D. Smet, G. W. Biedermann, J. Lee, and P. D. D. Schwindt, AVS Quantum Sci. **3**, 035001 (2021).
[106]A. T. Dellis, V. Shah, E. A. Donley, S. Knappe, and J. Kitching, Opt. Lett. **41**, 2775 (2016).
[107]J. A. Fedchak, J. K. Scherschligt, S. Avdiaj, D. S. Barker, S. P. Eckel, B. Bowers, S. O'Connell, and P. Henderson, J. Vac. Sci. Technol. B **39**, 024201 (2021).
[108]M. D. Lachmann, H. Ahlers, D. Becker, A. N. Dinkelaker, J. Grosse, O. Hellmig, H. Müntinga, V. Schkolnik, S. T. Seidel, T. Wendrich, A. Wenzlawski, B. Carrick, N. Gaaloul, D. Lüdtke, C. Braxmaier, W. Ertmer, M. Krutzik, C. Lämmerzahl, A. Peters, W. P. Schleich, K. Sengstock, A. Wicht, P. Windpassinger, and E. M. Rasel, Nat. Commun. **12**, 1317 (2021).
[109]C. Kürbis, A. Bawamia, M. Krüger, R. Smol, A. Peters, A. Wicht, and G. Tränkle, Appl. Opt. **59**, 253 (2020).
[110]M. Lezius, T. Wilken, C. Deutsch, M. Giunta, O. Mandel, A. Thaller, V. Schkolnik, M. Schiemangk, A. Dinkelaker, A. Kohfeldt, A. Wicht, M. Krutzik, A. Peters, O. Hellmig, H. Duncker, K. Sengstock, P. Windpassinger, K. Lampmann, T. Hülsing, T. W. Hänsch, and R. Holzwarth, Optica **3**, 1381 (2016).
[111]K. Döringshoff, F. B. Gutsch, V. Schkolnik, C. Kürbis, M. Oswald, B. Pröbster, E. V. Kovalchuk, A. Bawamia, R. Smol, T. Schuldt, M. Lezius, R. Holzwarth, A. Wicht, C. Braxmaier, M. Krutzik, and A. Peters, Phys. Rev. Appl. **11**, 054068 (2019).
[112]J. Pahl, A. N. Dinkelaker, C. Grzeschik, J. Kluge, M. Schiemangk, A. Wicht, A. Peters, and M. Krutzik, Appl. Opt. **58**, 5456 (2019).
[113]E. Luvsandamdin, C. Kürbis, M. Schiemangk, A. Sahm, A. Wicht, A. Peters, G. Erbert, and G. Tränkle, Opt. Express **22**, 7790 (2014).
[114]M. Schiemangk, K. Lampmann, A. Dinkelaker, A. Kohfeldt, M. Krutzik, C. Kürbis, A. Sahm, S. Spießberger, A. Wicht, G. Erbert, G. Tränkle, and A. Peters, Appl. Opt. **54**, 5332 (2015).
[115]A. Müller, J. Fricke, F. Bugge, O. Brox, G. Erbert, and B. Sumpf, Appl. Phys. B **122**, 87 (2016).
[116]V. Ménoret, P. Vermeulen, N. L. Moigne, S. Bonvalot, P. Bouyer, A. Landragin, and B. Desruelle, Sci. Rep. **8**, 12300 (2018).
[117]V. Ménoret, R. Geiger, G. Stern, N. Zahzam, B. Battelier, A. Bresson, A. Landragin, and P. Bouyer, Opt. Lett. **36**, 4128 (2011).
[118]B. Battelier, B. Barrett, L. Fouché, L. Chichet, L. Antoni-Micollier, H. Porte, F. Napolitano, J. Lautier, A. Landragin, and P. Bouyer, Proc. SPIE **9900**, 990004 (29 April 2016).
[119]S. Madkhaly, L. Coles, C. Morley, C. Colquhoun, T. Fromhold, N. Cooper, and L. Hackermüller, PRX Quantum **2**, 030326 (2021).
[120]H. Duncker, O. Hellmig, A. Wenzlawski, A. Grote, A. J. Rafipoor, M. Rafipoor, K. Sengstock, and P. Windpassinger, Appl. Opt. **53**, 4468–4474 (2014).
[121]M. Mihm, J. P. Marburger, A. Wenzlawski, O. Hellmig, O. Anton, K. Döringshoff, M. Krutzik, A. Peters, P. Windpassinger, and MAIUS Team, Acta Astronaut. **159**, 166–169 (2019).
[122]M. Christ, A. Kassner, R. Smol, A. Bawamia, H. Heine, W. Herr, A. Peters, M. C. Wurz, E. M. Rasel, A. Wicht, and M. Krutzik, CEAS Space J. **11**, 561–566 (2019).
[123]A. Krischke, M. Schulz, C. Knothe, and U. Oechsner, *Rugged, Modular and Fiber Coupled Beam Splitting and Combining Units* (Schäfter+Kirchhoff GmbH, Hamburg, 2020).
[124]I. Drougkakis, V. Tzardis, D. Pal, V. Pareek, G. Vasilakas, N. Papadakis, D. G. Papazoglou, and W. von Klitzing, Proc. SPIE **11852**, 2769 (11 June 2021).
[125]I. Drougkakis, K. G. Mavrakis, K. Poulios, G. Vasilakis, D. G. Papazoglou, and W. von Klitzing, Proc. SPIE **11180**, 1118053 (2019).
[126]S.-W. Chiow and N. Yu, Appl. Phys. B **124**, 96 (2018).
[127]S. Templier, J. Hauden, P. Cheiney, F. Napolitano, H. Porte, P. Bouyer, B. Barrett, and B. Battelier, Phys. Rev. Appl. **16**, 044018 (2021).
[128]B. Wiegand, B. Leykauf, K. Döringshoff, Y. D. Gupta, A. Peters, and M. Krutzik, Rev. Sci. Instrum. **90**, 103202 (2019).
[129]A. Strangfeld, S. Kanthak, M. Schiemangk, B. Wiegand, A. Wicht, A. Ling, and M. Krutzik, J. Opt. Soc. Am. B **38**, 1885 (2021).
[130]MuQuans/iXblue - ESA Contract No. 4000116740/16/NL/MP: Development of Cooling/Raman laser source with enhanced operational features.
[131]Z. L. Newman, V. Maurice, T. Drake, J. R. Stone, T. C. Briles, D. T. Spencer, C. Fredrick, Q. Li, D. Westly, B. R. Ilic, B. Shen, M.-G. Suh, K. Y. Yang, C. Johnson, D. M. S. Johnson, L. Hollberg, K. J. Vahala, K. Srinivasan, S. A. Diddams, J. Kitching, S. B. Papp, and M. T. Hummon, Optica **6**, 680 (2019).
[132]E. Imhof, B. K. Stuhl, B. Kasch, B. Kroese, S. E. Olson, and M. B. Squires, Phys. Rev. A **96**, 033636 (2017).
[133]E. L. Raab, M. Prentiss, A. Cable, S. Chu, and D. E. Pritchard, Phys. Rev. Lett. **59**, 2631 (1987).
[134]P. D. Lett, W. D. Phillips, S. L. Rolston, C. E. Tanner, R. N. Watts, and C. I. Westbrook, J. Opt. Soc. Am. B **6**, 2084 (1989).
[135]J. P. McGilligan, P. F. Griffin, R. Elvin, S. J. Ingleby, E. Riis, and A. S. Arnold, Sci. Rep. **7**, 384 (2017).
[136]A. S. Arnold, "Preparation and manipulation of an 87Rb Bose-Einstein condensate," Ph.D. thesis (University of Sussex, Brighton, 1999).
[137]L. Liu, D.-S. Lü, W.-B. Chen, T. Li, Q.-Z. Qu, B. Wang, L. Li, W. Ren, Z.-R. Dong, J.-B. Zhao, W.-B. Xia, X. Zhao, J.-W. Ji, M.-F. Ye, Y.-G. Sun, Y.-Y. Yao, D. Song, Z.-G. Liang, S.-J. Hu, D.-H. Yu, X. Hou, W. Shi, H.-G. Zang, J.-F. Xiang, X.-K. Peng, and Y.-Z. Wang, Nat. Commun. **9**, 2760 (2018).
[138]K. I. Lee, J. A. Kim, H. R. Noh, and W. Jhe, Opt. Lett. **21**, 1177 (1996).
[139]S. Pollock, J. P. Cotter, A. Laliotis, and E. A. Hinds, Opt. Express **17**, 14109 (2009).
[140]Q. Bodart, S. Merlet, N. Malossi, F. P. Dos Santos, P. Bouyer, and A. Landragin, Appl. Phys. Lett. **96**, 134101 (2010).
[141]A. Hinton, M. Perea-Ortiz, J. Winch, J. Briggs, S. Freer, D. Moustoukas, S. Powell-Gill, C. Squire, A. Lamb, C. Rammeloo, B. Stray, G. Voulazeris, L. Zhu, A. Kaushik, Y.-H. Lien, A. Niggebaum, A. Rodgers, A. Stabrawa, D. Boddice, S. R. Plant, G. W. Tuckwell, K. Bongs, N. Metje, and M. Holynski, Philos. Trans. R. Soc. A **375**, 20160238 (2017).
[142]W. Bowden, R. Hobson, I. R. Hill, A. Vianello, M. Schioppo, A. Silva, H. S. Margolis, P. E. G. Baird, and P. Gill, Sci. Rep. **9**, 11704 (2019).
[143]M. Vangeleyn, P. F. Griffin, E. Riis, and A. S. Arnold, Opt. Express **17**, 13601 (2009).
[144]M. Vangeleyn, P. F. Griffin, E. Riis, and A. S. Arnold, Opt. Lett. **35**, 3453 (2010).
[145]C. C. Nshii, M. Vangeleyn, J. P. Cotter, P. F. Griffin, E. A. Hinds, C. N. Ironside, P. See, A. G. Sinclair, E. Riis, and A. S. Arnold, Nat. Nanotechnol. **8**, 321 (2013).
[146]J. P. McGilligan, P. F. Griffin, E. Riis, and A. S. Arnold, Opt. Express **23**, 8948 (2015).
[147]J. P. McGilligan, P. F. Griffin, E. Riis, and A. S. Arnold, J. Opt. Soc. Am. B **33**, 1271 (2016).
[148]J. P. Cotter, J. P. McGilligan, P. F. Griffin, I. M. Rabey, K. Docherty, E. Riis, A. S. Arnold, and E. A. Hinds, Appl. Phys. B **122**, 172 (2016).
[149]R. Elvin, G. W. Hoth, M. Wright, B. Lewis, J. P. McGilligan, A. S. Arnold, P. F. Griffin, and E. Riis, Opt. Express **27**, 38359 (2019).
[150]S. Eckel, D. S. Barker, J. A. Fedchak, N. N. Klimov, E. Norrgard, J. Scherschligt, C. Makrides, and E. Tiesinga, Metrologia **55**, S182 (2018).
[151]J. Franssen, T. de Raadt, M. van Ninhuijs, and O. Luiten, Phys. Rev. Accel. Beams **22**, 023401 (2019).
[152]M. A. W. van Ninhuijs, K. A. Daamen, J. G. H. Franssen, J. Conway, B. Platier, J. Beckers, and O. J. Luiten, Phys. Rev. A **100**, 061801 (2019).
[153]H. Heine, "Grating MOT + magnetic chip trap," YouTube video (2021).
[154]D. Barker, E. Norrgard, N. Klimov, J. Fedchak, J. Scherschligt, and S. Eckel, Phys. Rev. Appl. **11**, 064023 (2019).
[155]A. Bregazzi, P. F. Griffin, A. S. Arnold, D. P. Burt, G. Martinez, R. Boudot, J. Kitching, E. Riis, and J. P. McGilligan, Appl. Phys. Lett. **119**, 184002 (2021).
[156]A. Sitaram, P. K. Elgee, G. K. Campbell, N. N. Klimov, S. Eckel, and D. S. Barker, Rev. Sci. Instrum. **91**, 103202 (2020).

[157]V. A. Henderson, M. Y. H. Johnson, Y. B. Kale, P. F. Griffin, E. Riis, and A. S. Arnold, Optics Express **28**, 9072 (2020).
[158]L. Amico, M. Boshier, G. Birkl, A. Minguzzi, C. Miniatura, L.-C. Kwek, D. Aghamalyan, V. Ahufinger, D. Anderson, N. Andrei, A. S. Arnold, M. Baker, T. A. Bell, T. Bland, J. P. Brantut, D. Cassettari, W. J. Chetcuti, F. Chevy, R. Citro, S. D. Palo, R. Dumke, M. Edwards, R. Folman, J. Fortagh, S. A. Gardiner, B. M. Garraway, G. Gauthier, A. Günther, T. Haug, C. Hufnagel, M. Keil, P. Ireland, M. Lebrat, W. Li, L. Longchambon, J. Mompart, O. Morsch, P. Naldesi, T. W. Neely, M. Olshanii, E. Orignac, S. Pandey, A. Pérez-Obiol, H. Perrin, L. Piroli, J. Polo, A. L. Pritchard, N. P. Proukakis, C. Rylands, H. Rubinsztein-Dunlop, F. Scazza, S. Stringari, F. Tosto, A. Trombettoni, N. Victorin, W. von Klitzing, D. Wilkowski, K. Xhani, and A. Yakimenko, AVS Quantum Sci. **3**, 039201 (2021).
[159]W. Hänsel, P. Hommelhoff, T. Hänsch, and J. Reichel, Nature **413**, 498 (2001).
[160]T. van Zoest, N. Gaaloul, Y. Singh, H. Ahlers, W. Herr, S. T. Seidel, W. Ertmer, E. Rasel, M. Eckart, E. Kajari, S. Arnold, G. Nandi, W. P. Schleich, R. Walser, A. Vogel, K. Sengstock, K. Bongs, W. Lewoczko-Adamczyk, M. Schiemangk, T. Schuldt, A. Peters, T. Könemann, H. Müntinga, C. Lämmerzahl, H. Dittus, T. Steinmetz, T. W. Hänsch, and J. Reichel, Science **328**, 1540 (2010).
[161]S. Amri, R. Corgier, D. Sugny, E. M. Rasel, N. Gaaloul, and E. Charron, Sci. Rep. **9**, 5346 (2019).
[162]S. Abend, M. Gebbe, M. Gersemann, H. Ahlers, H. Müntinga, E. Giese, N. Gaaloul, C. Schubert, C. Lämmerzahl, W. Ertmer, W. P. Schleich, and E. M. Rasel, Phys. Rev. Lett. **117**, 203003 (2016).
[163]A. Couvert, M. Jeppesen, T. Kawalec, G. Reinaudi, R. Mathevet, and D. Guéry-Odelin, Europhys. Lett. **83**, 50001 (2008).
[164]C. Vogt, M. Woltmann, S. Herrmann, C. Lämmerzahl, H. Albers, D. Schlippert, and E. M. Rasel, Phys. Rev. A **101**, 013634 (2020).
[165]K. S. Hardman, P. J. Everitt, G. D. McDonald, P. Manju, P. B. Wigley, M. A. Sooriyabandara, C. C. N. Kuhn, J. E. Debs, J. D. Close, and N. P. Robins, Phys. Rev. Lett. **117**, 138501 (2016).
[166]R. Roy, A. Green, R. Bowler, and S. Gupta, Phys. Rev. A **93**, 043403 (2016).
[167]S. Stellmer, R. Grimm, and F. Schreck, Phys. Rev. A **87**, 013611 (2013).
[168]K. Yamashita, K. Hanasaki, A. Ando, M. Takahama, and T. Kinoshita, Phys. Rev. A **95**, 013609 (2017).
[169]A. Urvoy, Z. Vendeiro, J. Ramette, A. Adiyatullin, and V. Vuletić, Phys. Rev. Lett. **122**, 203202 (2019).
[170]D. S. Naik, H. Eneriz-Imaz, M. Carey, T. Freegarde, F. Minardi, B. Battelier, P. Bouyer, and A. Bertoldi, Phys. Rev. Res. **2**, 013212 (2020).
[171]T. Vanderbruggen and M. W. Mitchell, Phys. Rev. A **87**, 033410 (2013).
[172]A fiber-based laser system (EDFA) will be validated with the CNES demonstrator No. Y-TSO/15-71.
[173]These challenges are currently investigated by the IQ O Hannover in cooperation with the institute of microproduction technology (IMPT) of LUH. Progress has been demonstrated within the ESA project "Compact Vacuum Chamber for an Earth Gravity Gradiometer Based on Laser-cooled Atom Interferometry" (ESA Contract No. 4000112182/14/NL/RA) and a prototype atom interferometer chip in a vacuum chamber is under development by RAL Space and IQO Hannover under ESA Contract.
[174]P. Asenbaum, C. Overstreet, T. Kovachy, D. D. Brown, J. M. Hogan, and M. A. Kasevich, Phys. Rev. Lett. **118**, 183602 (2017).
[175]M. Gebbe, J.-N. Siemß, M. Gersemann, H. Müntinga, S. Herrmann, C. Lämmerzahl, H. Ahlers, N. Gaaloul, C. Schubert, K. Hammerer, S. Abend, and E. M. Rasel, Nat. Commun. **12**, 2544 (2021).
[176]O. Carraz, R. Charrière, M. Cadoret, N. Zahzam, Y. Bidel, and A. Bresson, Phys. Rev. A **86**, 033605 (2012).
[177]S. Bade, L. Djadaojee, M. Andia, P. Cladé, and S. Guellati-Khelifa, Phys. Rev. Lett. **121**, 073603 (2018).
[178]N. Mielec, M. Altorio, R. Sapam, D. Horville, D. Holleville, L. A. Sidorenkov, A. Landragin, and R. Geiger, Appl. Phys. Lett. **113**, 161108 (2018).
[179]A. Trimeche, M. Langlois, S. Merlet, and F. Pereira Dos Santos, Phys. Rev. Appl. **7**, 034016 (2017).
[180]R. Karcher, A. Imanaliev, S. Merlet, and F. P. D. Santos, New J. Phys. **20**, 113041 (2018).
[181]E. Rocco, R. N. Palmer, T. Valenzuela, V. Boyer, A. Freise, and K. Bongs, New J. Phys. **16**, 093046 (2014).
[182]G. Santarelli, P. Laurent, P. Lemonde, A. Clairon, A. G. Mann, S. Chang, A. N. Luiten, and C. Salomon, Phys. Rev. Lett. **82**, 4619 (1999).
[183]G. Biedermann, X. Wu, L. Deslauriers, K. Takase, and M. A. Kasevich, Opt. Lett. **34**, 347 (2009).
[184]A. Sugarbaker, S. M. Dickerson, J. M. Hogan, D. M. S. Johnson, and M. A. Kasevich, Phys. Rev. Lett. **111**, 113002 (2013).
[185]Y. Cheng, K. Zhang, L.-L. Chen, T. Zhang, W.-J. Xu, X.-C. Duan, M.-K. Zhou, and Z.-K. Hu, Phys. Rev. A **98**, 043611 (2018).
[186]F. Sorrentino, A. Bertoldi, Q. Bodart, L. Cacciapuoti, M. de Angelis, Y.-H. Lien, M. Prevedelli, G. Rosi, and G. M. Tino, Appl. Phys. Lett. **101**, 114106 (2012).
[187]J. Lautier, L. Volodimer, T. Hardin, S. Merlet, M. Lours, F. Pereira Dos Santos, and A. Landragin, Appl. Phys. Lett. **105**, 144102 (2014).
[188]A. Peters, K. Y. Chung, and S. Chu, Metrologia **38**, 25 (2001).
[189]S. Loriani, C. Schubert, D. Schlippert, W. Ertmer, F. P. D. Santos, E. M. Rasel, N. Gaaloul, and P. Wolf, Phys. Rev. D **102**, 124043 (2020).
[190]G. T. Foster, J. B. Fixler, J. M. McGuirk, and M. A. Kasevich, Opt. Lett. **27**, 951 (2002).
[191]J. K. Stockton, X. Wu, and M. A. Kasevich, Phys. Rev. A **76**, 033613 (2007).
[192]A. Bonnin, N. Zahzam, Y. Bidel, and A. Bresson, Phys. Rev. A **92**, 023626 (2015).
[193]G. Rosi, L. Cacciapuoti, F. Sorrentino, M. Menchetti, M. Prevedelli, and G. Tino, Phys. Rev. Lett. **114**, 013001 (2015).
[194]A. Roura, Phys. Rev. Lett. **118**, 160401 (2017).
[195]G. D'Amico, G. Rosi, S. Zhan, L. Cacciapuoti, M. Fattori, and G. Tino, Phys. Rev. Lett. **119**, 253201 (2017).
[196]C. Overstreet, P. Asenbaum, T. Kovachy, R. Notermans, J. M. Hogan, and M. A. Kasevich, Phys. Rev. Lett. **120**, 183604 (2018).
[197]R. Caldani, K. X. Weng, S. Merlet, and F. Pereira Dos Santos, Phys. Rev. A **99**, 033601 (2019).
[198]C. Avinadav, D. Yankelev, O. Firstenberg, and N. Davidson, Phys. Rev. Appl. **13**, 054053 (2020).
[199]D. Yankelev, C. Avinadav, N. Davidson, and O. Firstenberg, Sci. Adv. **6**, abd0650 (2020).
[200]A. Louchet-Chauvet, T. Farah, Q. Bodart, A. Clairon, A. Landragin, S. Merlet, and F. P. D. Santos, New J. Phys. **13**, 065025 (2011).
[201]E. Wodey, D. Tell, E. M. Rasel, D. Schlippert, R. Baur, U. Kissling, B. Kölliker, M. Lorenz, M. Marrer, U. Schläpfer, M. Widmer, C. Ufrecht, S. Stuiber, and P. Fierlinger, Rev. Sci. Instrum. **91**, 035117 (2020).
[202]L. Botti, R. Buffa, A. Bertoldi, D. Bassi, and L. Ricci, Rev. Sci. Instrum. **77**, 035103 (2006).
[203]K. Xiao, L. Wang, J. Guo, M. Zhu, X. Zhao, X. Sun, C. Ye, and X. Zhou, Rev. Sci. Instrum. **91**, 085107 (2020).
[204]J. Vovrosh, G. Voulazeris, P. G. Petrov, J. Zou, Y. Gaber, L. Benn, D. Woolger, M. M. Attallah, V. Boyer, K. Bongs, and M. Holynski, Sci. Rep. **8**, 2023 (2018).
[205]A. Bertoldi, C.-H. Feng, H. Eneriz, M. Carey, D. S. Naik, J. Junca, X. Zou, D. O. Sabulsky, B. Canuel, P. Bouyer, and M. Prevedelli, Rev. Sci. Instrum. **91**, 033203 (2020).
[206]M. Yu, H. Cheng, Y. Meng, J. Wan, X. Wang, X. Ouyang, L. Xiao, and L. Liu, Rev. Sci. Instrum. **90**, 053203 (2019).
[207]P. Cheiney, L. Fouché, S. Templier, F. Napolitano, B. Battelier, P. Bouyer, and B. Barrett, Phys. Rev. Appl. **10**, 034030 (2018).
[208]S. Merlet, J. L. Gouët, Q. Bodart, A. Clairon, A. Landragin, F. P. D. Santos, and P. Rouchon, Metrologia **46**, 87 (2009).
[209]F. P. Dos Santos, Phys. Rev. A **91**, 063615 (2015).
[210]B. Barrett, L. Antoni-Micollier, L. Chichet, B. Battelier, P.-A. Gominet, A. Bertoldi, P. Bouyer, and A. Landragin, New J. Phys. **17**, 085010 (2015).
[211]I. Geisel, K. Cordes, J. Mahnke, S. Jöllenbeck, J. Ostermann, J. Arlt, W. Ertmer, and C. Klempt, Appl. Phys. Lett. **102**, 214105 (2013).
[212]R. Storn and K. Price, J. Global Optim. **11**, 341 (1997).
[213]J. M. Hogan, D. M. S. Johnson, and M. A. Kasevich, "Light-pulse atom interferometry," in *Atom Optics and Space Physics, Proceedings of the International School of Physics "Enrico Fermi,"* edited by E. Arimondo, W. Ertmer, and W. P. Schleich (IOS Press, Amsterdam, 2009), Vol. 168 pp. 411–447.
[214]K. Bongs, R. Launay, and M. Kasevich, Appl. Phys. B **84**, 599 (2006).
[215]G. Tino, L. Cacciapuoti, S. Capozziello, G. Lambiase, and F. Sorrentino, Prog. Part. Nucl. Phys. **112**, 103772 (2020).

[216]A. Bertoldi, F. Minardi, and M. Prevedelli, Phys. Rev. A **99**, 033619 (2019).
[217]C. Lotz, Y. Wessarges, J. Hermsdorf, W. Ertmer, and L. Overmeyer, Adv. Space Res. **61**, 1967 (2018).
[218]B. Reitz, C. Lotz, N. Gerdes, S. Linke, E. Olsen, K. Pflieger, S. Sohrt, M. Ernst, P. Taschner, J. Neumann, E. Stoll, and L. Overmeyer, Microgravity Sci. Technol. **33**, 25 (2021).
[219]L. Wacker, N. B. Jørgensen, D. Birkmose, R. Horchani, W. Ertmer, C. Klempt, N. Winter, J. Sherson, and J. J. Arlt, Phys. Rev. A **92**, 053602 (2015).
[220]R. H. Parker, C. Yu, W. Zhong, B. Estey, and H. Müller, Science **360**, 191 (2018).
[221]L. Morel, Z. Yao, P. Cladé, and S. Guellati-Khélifa, Nature **588**, 61 (2020).
[222]Naquidis is a regional innovation center in Quantum technology hosted at the Institut d'Optique d'Aquitaine, France. More information can be found at www.maquidis.com.

AFFILIATIONS

[1]Institut für Quantenoptik, Leibniz Universität Hannover, Welfengarten 1, 30167 Hannover, Germany
[2]Laboratoire Collisions Agrégats Réactivité (LCAR), Université Paul Sabatier, Bât. 3R1, 118 route de Narbonne, 31062 Toulouse Cedex 09, France
[3]Department of Physics, SUPA, University of Strathclyde, Glasgow G4 0NG, United Kingdom
[4]Institute of Physics, Bijeni ka cesta 46, 10000 Zagreb, Croatia
[5]School of Electronic Engineering, Dublin City University, Dublin 9, Ireland
[6]LP2N, Laboratoire Photonique, Numérique, Nanosciences, Université Bordeaux-IOGS-CNRS:UMR 5298, F-33400 Talence, France
[7]Ferdinand-Braun-Institut, Leibniz-Institut für Höchstfrequenztechnik, Gustav-Kirchhoff-Str. 4, D-12489 Berlin, Germany
[8]LNE-SYRTE, Observatoire de Paris, Université PSL, CNRS, Sorbonne Université, 61 avenue de l'Observatoire, 75014 Paris, France
[9]DPHY, ONERA, Université Paris-Saclay, Chemin de la Hunière, BP 80100, 91123 Palaiseau, France
[10]Van der Waals-Zeeman Institute, Institute of Physics, University of Amsterdam, Science Park 904, 1098XH Amsterdam, The Netherlands
[11]QuSoft, Science Park 123, 1098XG Amsterdam, The Netherlands
[12]Eindhoven University of Technology, Eindhoven, The Netherlands
[13]iXblue, Institut d'Optique d'Aquitaine, rue François Mitterrand, 33400 Talence, France
[14]Institute of Electronic Structure and Laser, Foundation for Research and Technology-Hellas, Heraklion 70013, Greece
[15]National Space Institute (DTU-Space), DTU Bldg 327, Elektrovej, DK-2800 Lyngby, Denmark
[16]AG Optische Metrologie, Institut für Physik, Humboldt-Universität zu Berlin, Newtonstraße 15, D-12489 Berlin, Germany
[17]Deutsches Zentrum für Luft- und Raumfahrt (DLR), Institut für Satellitengeodäsie und Inertialsensorik, Callinstr. 30b, 30167 Hannover, Germany
[18]Joint Lab Integrated Quantum Sensors, Institut für Physik, Humboldt-Universität zu Berlin, Newtonstraße 15, D-12489 Berlin, Germany
[19]Graz University of Technology, Rechbauerstraße 12, 8010 Graz, Austria
[20]Austrian Academy of Sciences, Space Research Institute, Schmiedlstraße 6, 8042 Graz, Austria
[21]Laboratoire Temps-Fréquence (LTF), Institut de Physique, Université de Neuchâtel, 2000 Neuchâtel, Switzerland
[22]ICFO-The Institute of Photonic Sciences, Av. Carl Friedrich Gauss, 3, 08860 Castelldefels, Barcelona, Spain and ICREA - Institució Catalana de Recerca i Estudis Avançats, 08010 Barcelona, Spain
[23]Thales Alenia Space, 26 Av. Jean François Champollion, 31100 Toulouse, France
[24]LNE-SYRTE, Observatoire de Paris, Université PSL, CNRS, Sorbonne Université, 61 avenue de l'Observatoire, 75014 Paris, France
[25]Airbus Defence and Space GmbH, Robert-Koch-Straße 1, 82024 Taufkirchen, Germany
[26]Dipartimento di Fisica e Astronomia and LENS Laboratory, Università degli Studi di Firenze, Istituto Nazionale di Fisica Nucleare, Sezione di Firenze-via Sansone 1, I-50019 Sesto Fiorentino (Firenze), Italy
[27]Institute of Physics, Faculty of Physics, Astronomy and Informatics, Nicolaus Copernicus University, Grudzia¸dzka 5, PL-87-100 Toruń, Poland